



70%

of surveyed scientists admitted that they could not replicate someone else's research.¹

50%

admitted that they couldn't replicate their own research.¹



Compact 1.8 cu.ft., stackable three high, with or without O₂ control.

Grow Cells Stress-Free Every Time

Improve Reproducibility in Clinical and Research Applications

Successful cell cultures require precise CO₂, O₂, temperature, humidity and real-time contamination protection maintained in PHCbi MCO-50 Series laboratory incubators. These compact incubators prevent contamination before it starts with standard inCu-safe® copper-enriched germicidal surfaces, easy clean integrated shelf channels and condensation control. H₂O₂ vapor and SafeCell™ UV scrubbing combine to increase *in vitro* cell safety.

Learn more at www.phchd.com/us/biomedical/cellculture-incubators

PHC Corporation of North America







PHC Corporation of North America
1300 Michael Drive, Suite A, Wood Dale, IL 60191
Toll Free USA (800) 858-8442, Fax (630) 238-0074
www.phchd.com/us/biomedical

¹) Baker, Morya. "1,500 scientists lift the lid on reproducibility." Nature, no. 533 (May 26, 2016): 452-54. doi:10.1038/533452a.

PHC Corporation of North America is a subsidiary of PHC Holdings Corporation, Tokyo, Japan, a global leader in development, design and manufacturing of laboratory equipment for biopharmaceutical, life sciences, academic, healthcare and government markets.

ARTICLE

Towards integrated production of an influenza A vaccine candidate with MDCK suspension cells

Thomas Bissinger¹  | Yixiao Wu^{1,2}  | Pavel Marichal-Gallardo¹  |
Dietmar Riedel³ | Xuping Liu⁴ | Yvonne Genzel¹  | Wen-Song Tan^{2,4}  |
Udo Reichl^{1,5} 

¹Bioprocess Engineering, Max Planck Institute for Dynamics of Complex Technical Systems, Magdeburg, Germany

²State Key Laboratory of Bioreactor Engineering, East China University of Science and Technology, Shanghai, China

³Facility for Transmission Electron Microscopy, Max Planck Institute for Biophysical Chemistry, Goettingen, Germany

⁴Shanghai BioEngine Sci-Tech Co., Shanghai, China

⁵Chair of Bioprocess Engineering, Otto von Guericke University Magdeburg, Magdeburg, Germany

Correspondence

Xuping Liu, Shanghai BioEngine Sci-Tech Co., 201203 Shanghai, China.

Email: liuxp@bio-engine.com.cn

Yvonne Genzel, Bioprocess Engineering Group, Max Planck Institute for Dynamics of Complex Technical Systems, 39106 Magdeburg, Germany.

Email: genzel@mpi-magdeburg.mpg.de

Present address

Thomas Bissinger, Roche Diagnostics GmbH, Pharma Research and Early Development, Bioprocess Research, Penzberg, Germany.

Abstract

Seasonal influenza epidemics occur both in northern and southern hemispheres every year. Despite the differences in influenza virus surface antigens and virulence of seasonal subtypes, manufacturers are well-adapted to respond to this periodical vaccine demand. Due to decades of influenza virus research, the development of new influenza vaccines is relatively straight forward. In similarity with the ongoing coronavirus disease 2019 pandemic, vaccine manufacturing is a major bottleneck for a rapid supply of the billions of doses required worldwide. In particular, egg-based vaccine production would be difficult to schedule and shortages of other egg-based vaccines with high demands also have to be anticipated. Cell culture-based production systems enable the manufacturing of large amounts of vaccines within a short time frame and expand significantly our options to respond to pandemics and emerging viral diseases. In this study, we present an integrated process for the production of inactivated influenza A virus vaccines based on a Madin–Darby Canine Kidney (MDCK) suspension cell line cultivated in a chemically defined medium. Very high titers of 3.6 log₁₀(HAU/100 µl) were achieved using fast-growing MDCK cells at concentrations up to 9.5 × 10⁶ cells/ml infected with influenza A/PR/8/34 H1N1 virus in 1 L stirred tank bioreactors. A combination of membrane-based steric-exclusion chromatography followed by pseudo-affinity chromatography with a sulfated cellulose membrane adsorber enabled full recovery for the virus capture step and up to 80% recovery for the virus polishing step. Purified virus particles showed a homogenous size distribution with a mean diameter of 80 nm. Based on a monovalent dose of 15 µg hemagglutinin (single-radial immunodiffusion assay), the level of total protein and host cell DNA was 58 µg and 10 ng, respectively. Furthermore, all process steps can be fully scaled up to industrial quantities for commercial manufacturing of either seasonal or pandemic influenza virus vaccines. Fast

Thomas Bissinger, Yixiao Wu, and Pavel Marichal-Gallardo contributed equally to this study.

This is an open access article under the terms of the Creative Commons Attribution-NonCommercial-NoDerivs License, which permits use and distribution in any medium, provided the original work is properly cited, the use is non-commercial and no modifications or adaptations are made.

© 2021 The Authors. *Biotechnology and Bioengineering* published by Wiley Periodicals LLC

production of up to 300 vaccine doses per liter within 4–5 days makes this process competitive not only to other cell-based processes but to egg-based processes as well.

KEYWORDS

chemically defined medium, downstream processing, influenza virus production, membrane chromatography, upstream processing

1 | INTRODUCTION

As for coronavirus disease 2019, influenza A virus (IAV) pandemics pose an unpredictable threat both for human health and global economies (Horimoto & Kawaoka, 2001; Kilbourne, 2006; Li et al., 2004). Several of the highly infectious IAV subtypes have the potential to develop pandemic strains spreading rapidly around the globe, causing severe damage to humans and animal livestock (Webby & Webster, 2003). Even though no influenza pandemic has been reported since 2009, preparedness to fight future local or global epidemics is needed (Fineberg, 2014; Girard et al., 2010; Webby & Webster, 2003). In case of a pandemic, vaccination will be the major control strategy to protect healthy individuals and to prevent further IAV distribution (Ferguson et al., 2006; Kostova et al., 2013). In such a scenario, billions of vaccine doses would be required at very short notice. Approved vaccines to battle seasonal influenza outbreaks come in three major formulations: live attenuated virus, inactivated virus (whole virus, split virus, and viral subunit), and recombinant viral surface antigen (hemagglutinin) (Bresee et al., 2018; Jin & Subbarao, 2015). Inactivated virus vaccines present the absolute majority (90%) of production capacity (Barr et al., 2018; Sparrow et al., 2021), thus playing a major role in vaccine manufacturing for a pandemic scenario (Stöhr, 2014). Here, either embryonated chicken eggs (ECE) or animal cells can be used as a substrate for influenza virus propagation. Even though egg-based flu vaccines dominate seasonal vaccine manufacturing, they are considered less suitable for pandemic influenza vaccine production (Audsley & Tannock, 2004). Apart from common disadvantages like long lead times for the start of manufacturing, poor scalability, and limitations in ECE supply (Genzel & Reichl, 2009), egg-derived vaccines might be less protective against some influenza virus strains (Raymond et al., 2016; Schild et al., 1983; Skowronski et al., 2014; Wu et al., 2017; Zost et al., 2017). In addition, ECEs are being used for a number of other vaccines, that is, to protect against yellow fever where frequent vaccine shortage has been reported (Centers for Disease Control and Prevention, 2020). In contrast, animal cell culture platforms are highly flexible, versatile, easily scalable, and can be very productive (Ernest & Kamen, 2015; Gallo-Ramirez et al., 2015). Especially with the application of single-use equipment, small production facilities could generate pandemic vaccines rapidly in the location of need (Coronel et al., 2019; George et al., 2010; Lopes, 2015). Several adherent and suspension cell lines were evaluated for influenza vaccine manufacturing, and among these, adherent Madin–Darby Canine Kidney

(MDCK) cells remain the most productive cell line (Genzel & Reichl, 2009). MDCK cells are easily accessible (Dukes et al., 2011), widely used in influenza research and already licensed successfully for vaccine manufacturing (Doroshenko & Halperin, 2009). For MDCK cells growing in suspension, however, disadvantages like low specific growth rate, low cell concentration, and unwanted formation of cell aggregates have been reported (Castro et al., 2015; Chu et al., 2009; Lohr et al., 2010; van Wielink et al., 2011). More recently, medium development led to fast-growing MDCK suspension cell lines with the capability to grow as single cells to concentrations exceeding 10×10^6 cells/ml (Bissinger et al., 2019; Huang et al., 2015; Wang et al., 2017). For large-scale manufacturing, both fast cell growth and high maximal cell density are crucial to reduce time to reach the needed production scale.

Besides production, virus particle purification plays a major role in the manufacturing of safe cell culture-based influenza vaccines (Onions et al., 2010). Biopharmaceutical products have to be purified to extremely high standards. Techniques for downstream processing (DSP) of virus particles at an industrial scale typically involve filtration and chromatography methods (Wolf & Reichl, 2011). Examples of the latter are ion-exchange chromatography (IEX) (Lee et al., 2015; Vajda et al., 2016), size exclusion chromatography (SEC) (Kröber et al., 2013; Yuan et al., 2015), hydrophobic interaction chromatography (Li et al., 2015; Wolff et al., 2010), affinity and pseudo-affinity chromatography (B. Carvalho et al., 2018; Fortuna et al., 2018), and multimodal chromatography (Baek et al., 2011; Kuiper et al., 2002). Standard unit operations, like depth filtration, (ultra-)centrifugation, (ultra-)filtration, and column chromatography are generally combined to build a DSP train (Morenweiser, 2005; Wolf & Reichl, 2011; Wolff & Reichl, 2008). Chromatography resins are porous bead-based stationary phases that have diffusional limitations and other mass transport disadvantages for the purification of large biomolecules (i.e., viruses) (Gagnon, 2010). In contrast, matrices with micron-sized flow channels that favor convective mass transport such as membranes and monoliths are much better suited for the purification of virus particles. Especially membrane-based chromatography materials are relatively inexpensive and allow single-use applications. Membrane-based steric exclusion chromatography (SXC) has been reported for the purification of IAV (Marichal-Gallardo et al., 2017). SXC is performed by mixing an unpurified solution containing virus particles with polyethylene glycol (PEG) and feeding this mixture into a chromatography column whose matrix consists of disposable cellulose membranes. The virus particles are captured on the membrane

surface without a direct chemical interaction, while smaller impurities are washed away. Selectivity in SXC is strongly based on the size of the target product and different influenza virus strains can be purified using the same process conditions. Unlike most other chromatography methods, in SXC the virus particles are loaded and eluted at physiological pH and salt concentrations that do not compromise the biological activity of the product. SXC can be complemented with pseudo-affinity chromatography using sulfated cellulose membrane adsorbers (SCMA) (Fortuna et al., 2018). Both SCMA and SXC have very high binding capacities and high recovery of influenza virus particles, which makes them perfect candidates for capture or polishing unit operations, respectively (Fortuna et al., 2018, 2019; Marichal-Gallardo et al., 2017; Opitz et al., 2009).

Although plenty of reports exist for either the production or the purification of cell culture-based influenza viruses, few integrated processes have been described in detail (Aggarwal et al., 2011; Genzel et al., 2006; Hu et al., 2011; Montomoli et al., 2012; Tree et al., 2001; Weigel et al., 2016). Moreover, despite many advantages of cell culture-based influenza vaccine manufacturing the application is still quite limited. This might be due to the high costs of process development, limitations of suitable cell lines for large-scale manufacturing, the lack of technological expertise, or the extremely high costs involved in the clinical testing of vaccine candidates. To overcome the technical limitations, careful analysis is crucial to demonstrate integrated process performance, robustness, and productivity. In this study, we present a workflow for integrated cell culture-based production and purification of an inactivated influenza vaccine candidate that involves batch cultivation of MDCK suspension cells in three parallel lab-scale stirred tank bioreactors in chemically defined medium and infection of cells with the influenza virus A/PR/8/34 H1N1 strain. We show the dynamics of cell growth, metabolism, and virus replication, the identification of the optimal harvest point, and a purification train including enzymatic digestion of the host cell DNA and membrane-based chromatography of harvested virus particles by capture with SXC and polishing with SCMA. Additionally, we examine intermediate process steps such as the chemical inactivation of virus particles and discuss the selection and combination of these unit operations for the whole process. Very detailed analytics are applied to analyze the integrated process with a comprehensive data set.

Overall, we demonstrate a comprehensive integrated platform technology with high potential for timely and fast large-scale manufacturing of pandemic influenza virus vaccines.

2 | MATERIAL AND METHODS

2.1 | Cell lines and cell culture

An MDCK suspension cell line (ATCC CCL-34 origin) adapted to grow in suspension in a serum-free medium (Huang et al., 2011, 2015; Wu et al., 2020), was cultivated in a newly developed chemically defined medium, referred as "Xeno-CDM" (Shanghai BioEngine Sci-Tech). For media adaptation to Xeno-CDM the medium proportion was increased

by 25% steps for four passages, with no apparent changes in cell line performance. MDCK suspension cells in Xeno-CDM were growing as single-cell suspension to maximal cell concentrations (batch) of up to 12×10^6 cells/ml (Figure S4). For small-scale cultivation, MDCK cells were grown in shake flasks (125/250 ml polycarbonate Erlenmeyer flask, #431143/#431144, Corning®) with 30/60 ml working volume (wv) in a Multitron Pro incubator (Infors HT) at 37°C and 5% CO₂ atmosphere with a shaking frequency of 100 rpm. Cells were passaged every 3 days with a seeding density of 0.5×10^6 cells/ml. Cell concentration, cell diameter, and cell viability were measured with a Vi-CELL XR automated cell counter (#731050, Beckman Coulter). The average cell volume was determined from the diameter size distribution (class width 0.31 µm) of the analyzed population (2000–15,000 cells) assuming a spherical cell shape. The viable cell volume (VCV) was calculated from average cell volume and viable cell concentration (VCC). For process evaluation, MDCK cells were cultivated in DASGIP® Bioreactors (#76DS0700DSS, Eppendorf) with 300–600 ml wv. Approximately 50 ml of independent precultures (Erlenmeyer flask, 60 ml wv, $8\text{--}9 \times 10^6$ cells/ml) were used to inoculate each bioreactor (STR1–3) with an initial wv of 400 ml at a cell concentration of 1×10^6 cells/ml. All bioreactors were controlled by a DASGIP® Parallel Bioreactor System (#76DG04CC, Eppendorf) using the DASware® control software (#76DGCS, Eppendorf). A macro-sparger with an air-oxygen mixture was used for aeration. The pH was controlled by CO₂ flow to the sparger and by the addition of 1 M NaOH. For agitation, a single 30° pitched 3-blade stirrer (O.D. 50 mm) was used at a stirring speed of 80 rpm.

2.2 | Influenza virus infection

All infections were carried out using an influenza A seed virus strain A/PR/8/34 of the subtype H1N1 from the Robert Koch Institute, named here thereafter either "IAV" or "APR8." The original seed virus propagated in adherent MDCK cells (#84121903, ECACC, Public Health) was adapted over five passages (multiplicity of infection [MOI] 10^{-5}) to the MDCK suspension cell line. For infection, MDCK cells were diluted by half with fresh Xeno-CDM with trypsin addition (final activity 30 U/ml; #27250018, Thermo Fisher Scientific). Seed virus (infectious titer of 1.8×10^9 TCID₅₀/ml) was diluted with phosphate-buffered saline (PBS) and added to the cell suspension with an MOI of 10^{-3} .

2.3 | Harvest and chemical inactivation of virus particles

A volume of 50 ml of cell suspension from each bioreactor was harvested at time points 18, 21, 24, 27, 30, and 36 h postinfection (hpi). Cells and debris were removed by centrifugation (800×g, 10 min, 4°C) and the supernatant ("virus harvest") was clarified by 0.45 µm filtration (Minisart, SFCA, #16555, Sartorius Stedim Biotech) ("clarified virus harvest"). An enzymatic DNA digestion was made

with an unspecific nuclease by supplementing the clarified virus harvest with magnesium chloride (#M8266-1KG; Sigma-Aldrich Chemie GmbH) to a final concentration of 2 mM and 10 U/ml Denarase® (named "Denarase" hereafter, #2DN100KU99; Sartorius Stedim Biotech). The sample was incubated under mixing for 24 h at 37°C. The clarified virus harvest was chemically inactivated either before or after the DNA digestion using beta-propiolactone (BPL, #33672.01; Serva Electrophoresis) added to a final concentration of 6 mM and incubated at 37°C for 24 h. The inactivated clarified virus harvest was filtered (Minisart, 0.22 µm, SFCA, #16534, Sartorius Stedim Biotech; Göttingen, Germany) and stored at -80°C until further processing.

2.4 | Chromatographic purification of virus particles

All chromatography experiments were performed with an ÄKTA Pure 25 (GE Healthcare) liquid chromatography system. The UV absorbance was monitored at 280 nm and virus particles were monitored with a NICOMPTM 380 (Particle Sizing Systems) submicron particle analyzer at 632.8 nm. All chromatography experiments were performed at room temperature.

Virus capture was done with membrane-based SXC as previously reported (Marichal-Gallardo et al., 2017). Inactivated clarified virus harvests were conditioned before SXC to a final concentration of 8% PEG-6000 (#81260-5KG; Sigma-Aldrich Chemie GmbH) using a 32% PEG-6000 stock solution. The SXC column comprised a stack of 1.0 µm regenerated cellulose membranes (#10410014; GE Healthcare) (20 layers; 100 cm² total surface) fitted into commercial 25 mm stainless steel filter housings as described before. The flow rate used was 10–15 ml/min. The SXC purifications were performed in bind-elute mode. Briefly, (a) equilibration: the column was washed with 10 column volumes (CV) of water followed by 10 CV of "SXC equilibration buffer" (50 mM Tris-HCl, 150 mM sodium chloride, 8% PEG-6000, pH 7.4). (b) Sample injection: the sample was then loaded onto the column followed by a wash step with equilibration buffer until baseline UV absorbance was achieved. (c) Elution: virus particles were recovered by washing with up to 25 CV of Tris buffer (50 mM Tris-HCl, 150 mM sodium chloride, pH 7.4).

The SXC elution pools were subsequently purified by pseudo-affinity chromatography using an SCMA as previously reported (Fortuna et al., 2018). Commercial sulfated cellulose membranes (94SC-04-001#; Sartorius Stedim Biotech) were fitted into the same filter housings used for SXC as described above (10 layers; 50 cm² total surface). The flow rates used were 10–15 ml/min. The polishing of SXC-purified influenza virions with SCMA was equally carried out in bind-elute. Briefly, (a) Equilibration: the column was washed with 10 CV of water followed by 10 CV of "SCMA equilibration buffer" (10 mM Tris-HCl, 4 mM NaCl, pH 7.4). (b) Sample injection: the sample was then loaded onto the column followed by a wash step with equilibration buffer until baseline UV absorbance was achieved. (c) Elution: virus particles were recovered by washing with 20 CV of

"SCMA elution buffer" (10 mM Tris-HCl, 1.0 M NaCl, pH 7.4). Elution fractions from either the SXC or SCMA purification steps were optionally dialyzed with 300 kDa molecular weight cut-off (MWCO) membranes as described previously (Marichal-Gallardo et al., 2017). Dialyzed samples were spiked with sucrose at a final concentration of 1% before freezing at -80°C. Additionally, SEC experiments were carried out with a packed-bead Superdex 200 Increase 10/300 GL column (#17517501; GE Healthcare). The sample injection volumes ranged from 50 to 500 µl and the flow rate was 0.75 ml/min.

2.5 | Sample preparation

The cell suspension was centrifuged at 800×g for 10 min at room temperature to remove cells and cell debris. The cell-free supernatant was aliquoted and stored at -80°C until respective analysis. For quantitation of metabolites, virus-containing samples were thawed and inactivated in a heat block at 80°C for 2 min before analysis.

2.6 | Quantitation of extracellular metabolites and osmolality

Concentration of glucose, glutamate, lactate, and ammonium were measured using a BioProfile 100 Plus analyzer (Nova Biomedical) using three external standards each. Glutamine was quantified with a Glutamine V2 Bio kit (#07395655001, Roche Diagnostics) using a Cedex Bio Analyzer (#06395554001, Roche Diagnostics). Amino acid concentrations were determined with the "UPLC Amino Acid Analysis Solution" using an ACQUITY UPLC H-Class (#720003294en, Waters). Medium osmolality was measured off-line with a vapor pressure osmometer (VAPRO® 5520, Wescor).

2.7 | Infectious virus titer by TCID₅₀ assay

For the quantification of infectious IAV particles a TCID₅₀ assay was used as described by Genzel and Reichl (2007). Cell-free, sterile supernatant was stored until measurement at -80°C. Confluent adherent MDCK cells (#84121903, ECACC, Public Health) cultivated in 96-well plates (GMEM medium) were infected with a serial dilution of virus samples (100 µl) and incubated for 48 h (37°C, 5% CO₂). MDCK cells were fixed with an ice-cold acetone solution (80%), stained with an anti-influenza A/PR/8/34 H1N1 HA serum (#03/242, NIBSC) and an Alexa Fluor donkey anti-sheep IgG antibody (#A11015, Thermo Fisher Scientific) as a secondary fluorescence label. Fluorescence positive and negative wells were counted using a fluorescence microscope (Axio Observer A1, Zeiss) and infectious titer was calculated from eight replicates with the Spearman-Kärber method (Kärber, 1931; Spearman, 1909). The infectious virus titer is expressed as TCID₅₀/ml.

2.8 | Virus titer by hemagglutination activity assay

Total influenza virus content was estimated by a hemagglutination activity (aHA) assay as described previously (Kalbfuss et al., 2008). Virus samples and standards were serially diluted in two dilution rows ($2^{(1-n)}$ and $2^{(0.5-n)}$ with n : 1–12) with PBS in 96-round-bottom-wells. A volume of 100 μ l of chicken erythrocyte solution was added (2×10^7 erythrocytes/ml) to diluted samples (100 μ l) and incubated for 3–8 h at room temperature. The aHA was evaluated using a plate reader (Infinite® M200 microplate reader, Tecan Group) measuring the extinction at 700 nm and the final titer was calculated by a curve fitting function of the resulting extinction data. The aHA titer is expressed as common logarithm (\log_{10}) of the hemagglutination units (HAUs) per analysis volume (100 μ l): $\log_{10}(\text{HAU}/100 \mu\text{l})$. For mass balancing in DSP and further calculations, the HA titer is also expressed in its linear form as HAUs per analysis volume (100 μ l): $\text{HAU}/100 \mu\text{l}$. From this, the corresponding total concentration of virus particles was estimated as follows:

$$\frac{\text{Virus}_{\text{total}}}{\text{ml}} = 2E7 \frac{1}{\text{ml}} \times \text{HAU} = 2E7 \frac{1}{\text{ml}} \times 10^{\log_{10}(\text{HAU}/100 \mu\text{l})} \quad (1)$$

2.9 | Virus antigen quantitation by single-radial immunodiffusion assay

The amount of the viral hemagglutinin (HA) surface antigen was quantified by a single-radial immunodiffusion (SRID) assay as previously reported (Wood et al., 1977). Samples were dialyzed as described before (Marichal-Gallardo et al., 2017) and lyophilized using 1% sucrose as cryo-protectant. Resuspension was made by adjusting the HA content of the samples to the HA content of a reference standard produced in-house as described by Opitz et al. (2009). The assay setups consisted of a 7×7 diffusion matrix made of a 1% agarose gel with 64 μ g/ml anti A/PR/8 antigen (#03/242; NIBSC). Values are reported in $\mu\text{g}_{\text{HA}}/\text{ml}$.

2.10 | Imaging flow cytometry

The relative amount of infected and apoptotic cells was determined by imaging flow cytometry, as described previously (Frensing et al., 2016). For cell fixation, 1 ml of infected MDCK cells were mixed with paraformaldehyde to a final concentration of 2% and incubated at 4°C for 30 min. Cells were washed with PBS (300 \times g, 10 min, 4°C), added to 5 ml cold (–20°C) 70% ethanol and stored at –20°C. For staining, fixed cells in ethanol were spun down (300 \times g, 10 min, 4°C) to remove storage solution. The cell pellet was washed twice with fluorescence activated cell sorting (FACS)-buffer (PBS containing 0.1% bovine serum albumin [BSA] and 2% glycine) and blocked in PBS containing 1% BSA (30 min, 37°C). vRNP positive cells were stained with a monoclonal mouse anti-NP antibody mAb61A5 (Momose et al., 2007) as a primary antibody, and Alexa Fluor 647-conjugated goat antimouse pAb (#A21235, Thermo Fisher Scientific) as a secondary antibody. All antibodies were incubated for 60 min at

37°C in FACS-buffer. Between each incubation step, cells were washed twice with FACS-buffer (300 \times g, 10 min, 4°C). Shortly before the analysis, nucleic DNA was stained with 4',6-diamidino-2-phenylindole. Ten thousand single cells were analyzed with an ImageStream X Mark II (#100220, Merck) using a $\times 60$ objective lens. Image analysis was carried out with the IDEAS software (version 6.1). The vRNP-positive cells were considered infected and nucleic condensation and fragmentation were considered a sign of apoptosis.

2.11 | Quantitation of total protein and host cell DNA

Total protein was estimated using a Bradford BioRad assay (#5000006; BioRad Laboratories). The calibration curve was made with BSA (#A3912; Sigma-Aldrich Chemie GmbH) in the range of 5–40 μ g/ml with a limit of detection (LOD) of 0.4 μ g/ml. The concentration of dsDNA was estimated with a Quant-iT™ PicoGreen assay (#P7581; Life Technologies GmbH). The standard curve was made with lambda DNA (# D1501; Promega) for the range of 4–250 ng/ml with LOD of 1.6 ng/ml. This assay is referred as “PicoGreen” hereafter.

2.12 | Particle size distribution by differential centrifugal sedimentation

Differential centrifugal sedimentation (DCS) analysis was performed using a CPS DC24000 UHR disc centrifuge (CPS Instruments Inc.) at 24,000 rpm with a 4%–16% (m/v) sucrose gradient in 50 mM Tris, 150 mM NaCl, pH 7.4 buffer, as reported previously (Pieler et al., 2017). Briefly, the gradient consisted of nine 1.6 ml steps with different sucrose concentrations each, that is, 16%, 14.5%, 13%, 11.5%, 10%, 8.5%, 7%, 5.5%, and 4% sucrose (m/v), with a total volume of 14.4 ml. The gradient quality was evaluated by injecting a 239 nm particle standard (0.3%–0.5% solid content, polyvinyl chloride, CPS Instruments Inc.) directly after gradient injection. Then, the gradient was equilibrated for 10 min, followed by another 239 nm particle standard injection for measurement calibration. Finally, 100 μ l of sample (1:1) were injected for the size distribution measurements of chromatography elution fractions. Additional density parameters for solutions and particles introduced into the software were 1.072 g/ml for the gradient buffer, 1.385 g/ml for the calibration particles, and 1.180 g/ml for IAV. The particle size distributions are displayed as normalized weight average in percentage against apparent hydrodynamic diameter in nm.

2.13 | Transmission electron microscopy

Transmission electron microscopy (TEM) of virus particles was done by negative staining. A solution containing virions was applied to glow-discharged carbon coated 400 mesh copper grids and stained

with 1% uranyl acetate. Virions were adsorbed to a continuous carbon film, attached to a Quantifoil (3.5/1) (Quantifoil) grid, and freeze-plunged in a Leica EM GP (Leica) employing the blotting sensor at 75% humidity and -24°C . Images were taken in a Philips CM120 electron microscope (Philips Inc.) using a TemCam F416 CMOS camera (TVIPS).

3 | RESULTS

3.1 | Optimization of stirred tank bioreactor cultivations

In preliminary studies, various cultivation conditions and infection parameters were evaluated for the cell growth and virus production phase in shake flasks and stirred tank bioreactors (STR). In particular, different agitation speeds from 80 rpm to 140 rpm were tested for suspension MDCK cultivation in the DASGIP system (Figure S4). Based on results obtained for cell growth, a stirring speed of 80 rpm was selected for subsequent process evaluations (data not shown). The pH control setpoints for the cell growth phase and the virus

infection phase were 7.00 and 7.20, respectively. Furthermore, based on scouting experiments in shake flasks, an MOI of 10^{-3} and a final trypsin concentration of 30 U/ml were used. For process evaluation, cell growth dynamics, viable cell concentration and cell volume, viability, and virus yields were monitored in three parallel bioreactors (STR1–3).

3.2 | Cell growth phase

With the used cultivation conditions, excellent growth of the MDCK suspension cell line adapted to Xeno-CDM was observed. After a short lag phase, cells grew exponentially within 3 days to a concentration of $9.5 \pm 0.5 \times 10^6$ cells/ml (Figure 1a). While cell diameters and cell concentrations showed some slight variations between batches after inoculation and in the last 24 h of the cell growth phase (Figures 1a and 1d), the viable cell volume was rather consistent between batches (Figure 1b). The average maximal value was 14.7 ± 0.5 $\mu\text{L}/\text{mL}$. Based on the viable cell volume, uptake and release rates for the main metabolites were determined as shown in the supplementary (Figure S2).

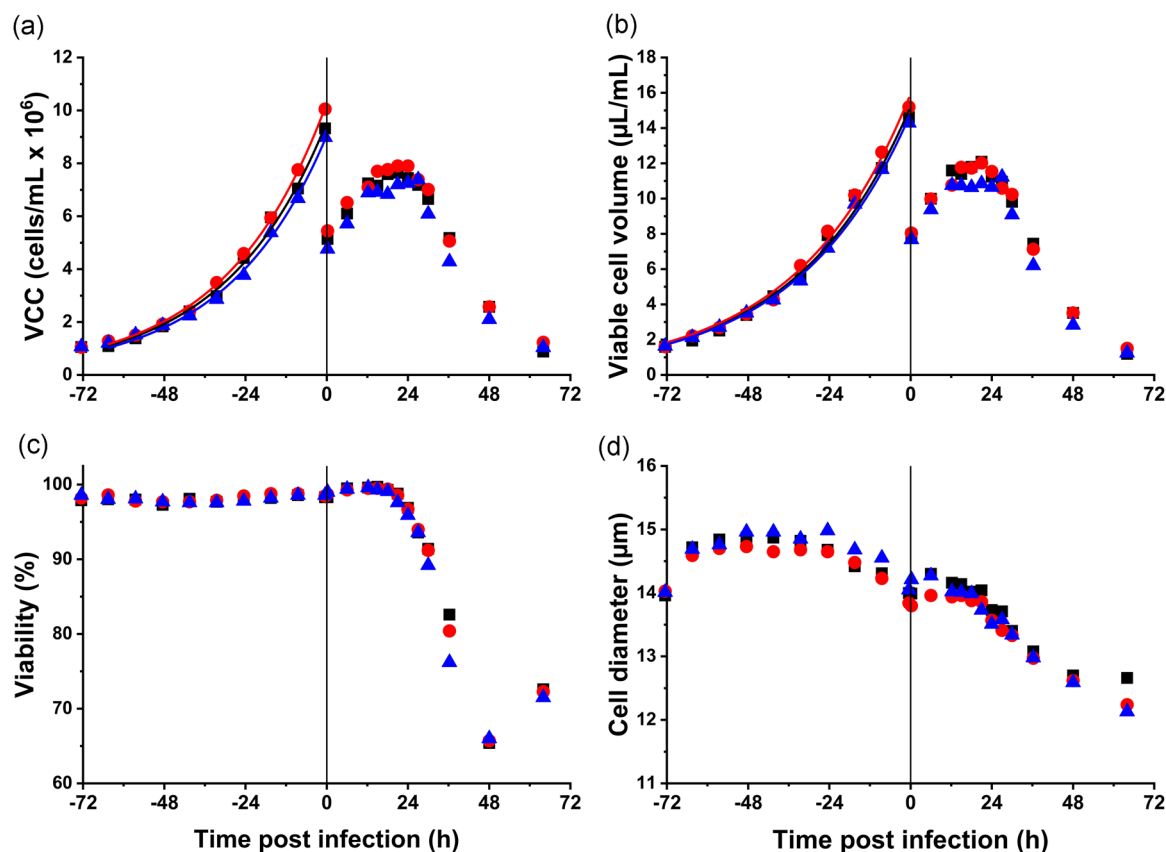


FIGURE 1 MDCK suspension cells cultivated in three parallel bioreactors for IAV production.

Viable cell concentration (a), viable cell volume (b), viability (c), and average cell diameter (d) were monitored over the whole process time (144 h). Cell concentrations (a) and cell volumes (b) were fitted to an exponential growth function (curves) to determine the specific growth rate. Vertical lines indicate time of infection, where cell suspension was diluted by half. STR1 (■), STR2 (●), STR3 (▲). IAV, influenza A virus; MDCK, Madin–Darby Canine Kidney

Fitting of exponential growth functions to cell concentrations and cell volumes (Figure 1b) resulted in an average specific growth rate of $\mu = 0.033 \text{ h}^{-1}$ (8–72 h) and $\mu = 0.031 \text{ h}^{-1}$ (0–72 h) for cell concentrations and cell volumes, respectively. Over the whole-cell growth phase cell viability was consistently high (>97%) and even increased slightly towards the end of the growth phase (>98%). No limitations were found for neither the main extracellular metabolites (Figure 2a,b) nor for most amino acids (Figures 3 and S3). Only the amino acids leucine, isoleucine, and methionine were below the limit of quantification at the end of the growth phase (Figure 3d–f). Cultivation and infections performed with higher initial leucine, isoleucine, and methionine concentrations neither increased cell concentration nor virus titer (data not shown). Accumulation of the by-products lactate and ammonium (Figure 2c,d) was expected but concentrations remained in a reasonable range where negative effects on metabolism or cell growth likely do not play a significant role (Gagnon et al., 2011; Schneider et al., 1996; Slivac et al., 2010). In addition to lactate and ammonium, the amino acids glutamate, alanine, and to a lesser extent aspartate, were produced (Figure 3a–c), presumably as by-products of the cellular transamination in glutamine metabolism (Eagle, 1959; Schneider et al., 1996).

3.3 | Infection phase

For infection, cells were diluted by half to approximately 5×10^6 cells/ml by adding fresh medium containing IAV for a final MOI of 10^{-3} . Trypsin activity was adjusted to 30 U/ml. MDCK cells continued to grow after infection reaching a maximal viable cell concentration of approximately 7×10^6 cells/ml at 21 hpi (Figure 1a). Afterward, the cell concentration started to decrease. Cell viability initially increased slightly (99%) but also started to decrease with the onset of virus accumulation (>21 hpi) (Figure 1c). Similarly, cell diameters decreased significantly during virus production (Figure 1d), due to virus-induced apoptosis and cell lysis. In contrast to the reduction in cell size during the growth phase (reduced osmolality), medium osmolality increased due to lactate release (Figure 2c) and base addition for pH control (Figure S1a). With the medium addition and the increase in working volume at the time of infection, cellular nutrients were replenished and by-products diluted. Similar to the growth phase, no significant limitation of main metabolites (Figure 2) and most analyzed amino acids (Figures 3 and S3) were found in the infection phase. As for the growth phase, isoleucine and methionine were below the limit of quantification (>18 hpi). As expected, uptake and release rates of main metabolites and by-products increased

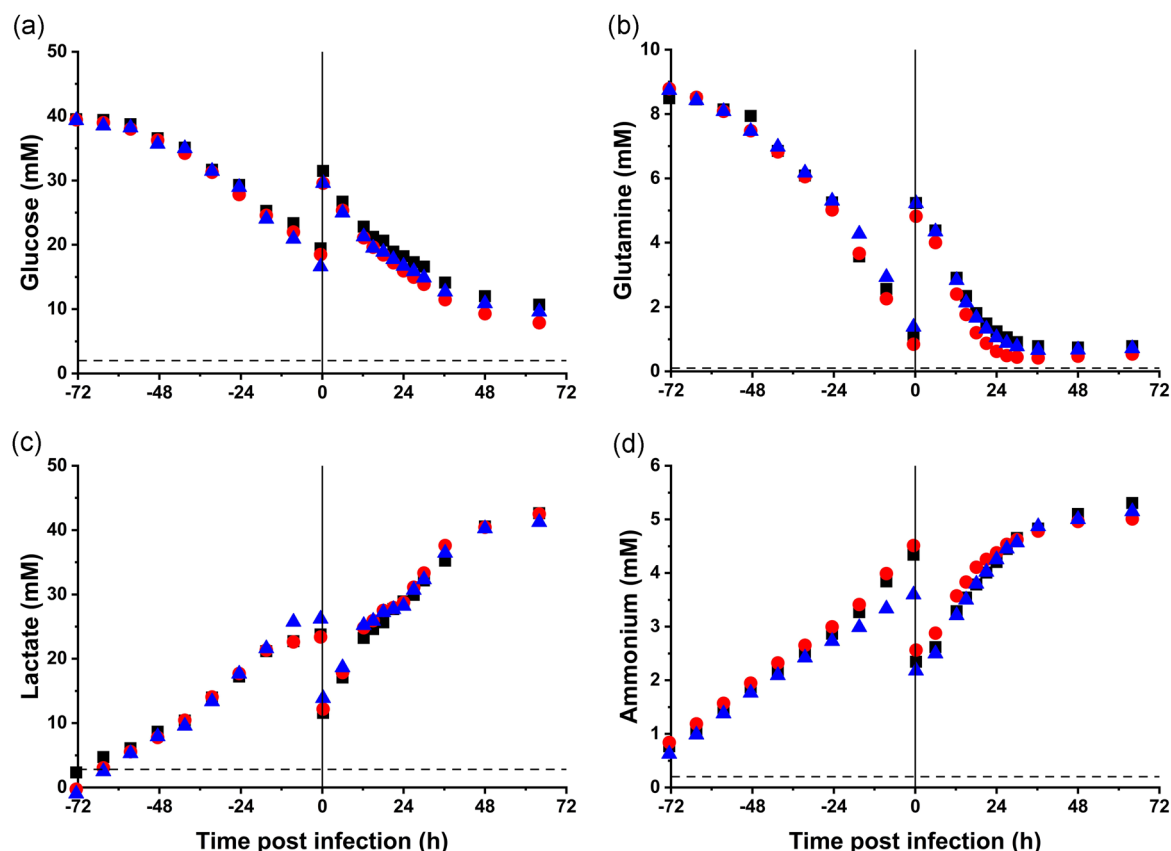


FIGURE 2 Main extracellular metabolites in three parallel bioreactors for influenza A virus production. Concentration of the main metabolites glucose (a), glutamine (b), lactate (c), and ammonium (d) in the cell culture medium over the processing time (144 h). Vertical lines indicate the time point of infection. Horizontal dashed lines indicate the limit of quantification of the respective metabolite. STR1 (■), STR2 (●), STR3 (▲)

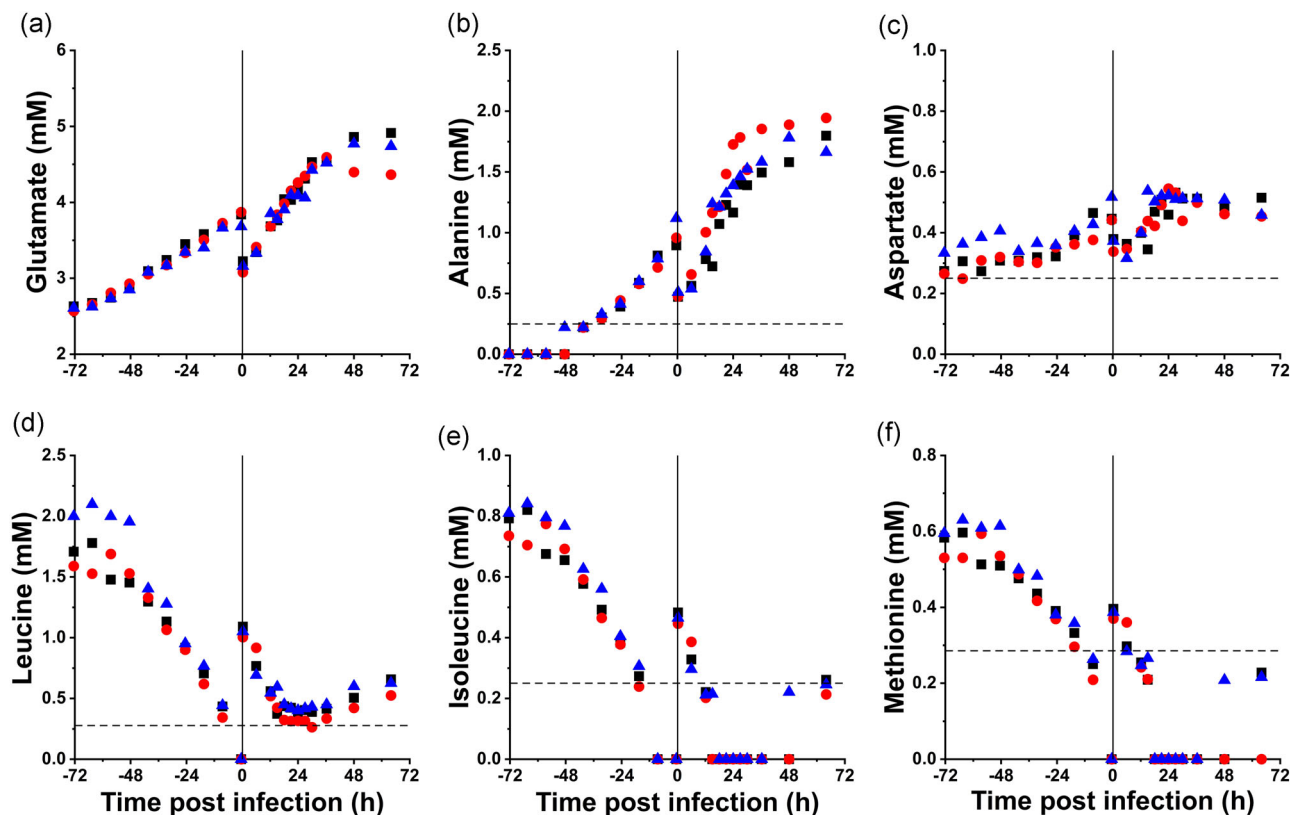


FIGURE 3 Concentration of selected amino acids in three parallel bioreactors for influenza A virus production.

Extracellular concentration of the amino acids glutamate (a), alanine (b), aspartate (c), leucine (d), isoleucine (e), and methionine (f) in the cell culture medium over the processing time (144 h). Vertical lines indicate the time point of infection. Horizontal dashed lines indicate the limit of quantification of the respective amino acid. STR1 (■), STR2 (●), STR3 (▲)

significantly immediately after addition of fresh medium (Figure S2). Later, the rate of glucose uptake and lactate release decreased while the rates for glutamine and ammonium remained rather constant (until about 15 hpi). With the full infection of the cell population at 15–18 hpi (Figure 4c) cells consumed more glucose and produced more lactate, but glutamine consumption and ammonium production declined rapidly (Figure S2). Lactate continued to accumulate and exceeded 40 mM at the end of infection phase.

Combining image stream analysis and virus quantification assays enabled to follow the virus replication dynamics. Fast virus replication led to an early increase in TCID₅₀ values and the percentage of infected cells, with a maximum at 18–27 hpi and 15–18 hpi, respectively (Figure 4b,c). A maximal infectious virus titer of $2.7 \pm 0.5 \times 10^9$ TCID₅₀/ml (21 hpi) was measured, followed by a titer reduction due to degradation of infectious virus particles (>27 hpi). A significant accumulation of aHA was not detected until 12 hpi, at which point it increased rapidly and plateaued (27 hpi) at $3.66 \pm 0.06 \log_{10}(\text{HAU}/100 \mu\text{l})$ (Figure 4a). With the infection spreading over the entire cell population, the percentage of apoptotic cells started to increase 12 hpi and reached a maximum (~80%) at the end of the infection phase (Figure 4d).

3.4 | Identification of the optimal harvest point

Manufacturing processes for biopharmaceuticals require an adequate integration of USP and DSP operations to reduce process time and costs. In addition, it is advantageous to minimize the contamination level for subsequent purification steps. Following the increase in virus titers, we observed a significant increase in the total protein and DNA concentration of the cell-free supernatant. While the total protein concentration increased only about fivefold, the DNA level increased by two orders of magnitude compared to the DNA concentration measured in the cell growth phase (Figures 5a and 5c). Total protein concentration started to increase already during the cell growth phase and increased rapidly at a later time of infection due to virus release (viral proteins) and virus-induced cell death (host cell proteins) (Figure 5a). In contrast, the level of host cell DNA remained more or less stable (100 ng/ml) during the cell growth phase but increased strongly after trypsin addition (time of infection). Most likely, the addition of trypsin led to the lysis of necrotic cells resulting in a slight increase in cellular viability (>99%) and the release of cellular DNA. At a later stage of infection, very high levels of DNA (> 2 µg/ml) were measured due to extensive virus-induced apoptosis and cell death (Figure 5c).

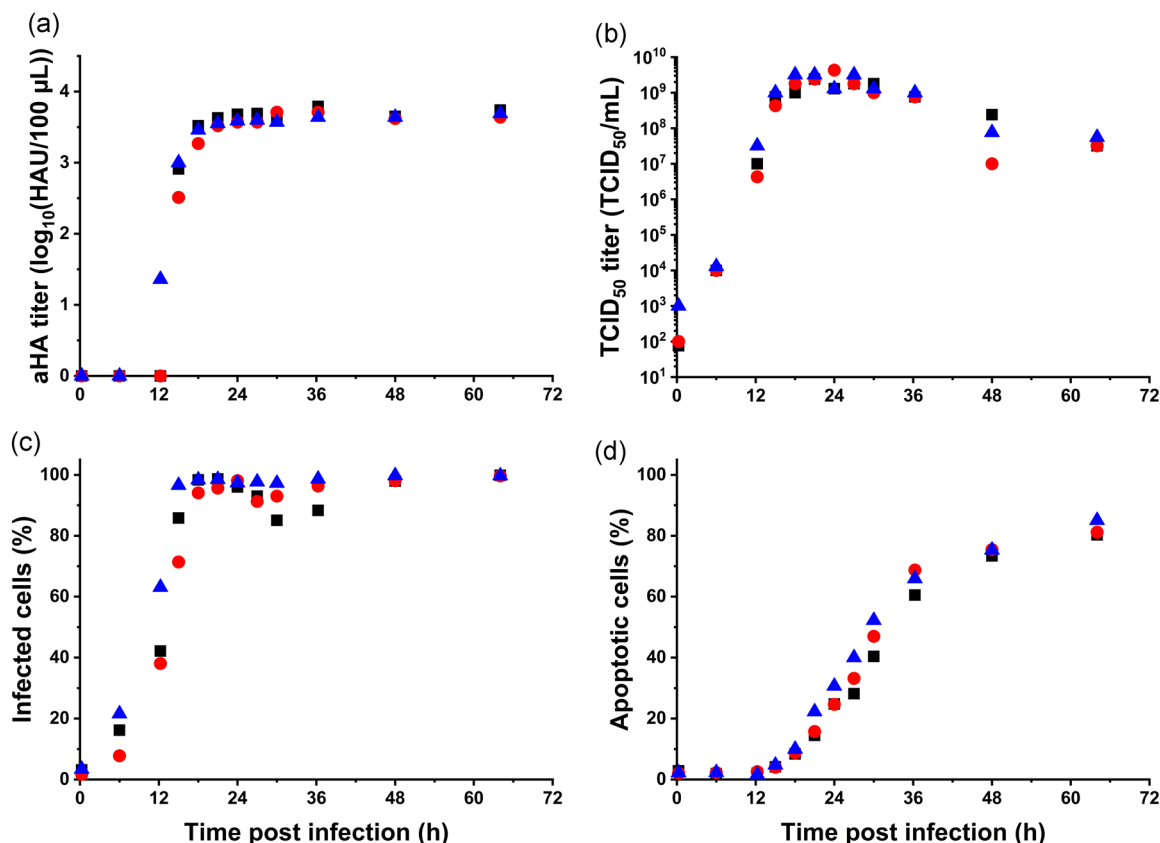


FIGURE 4 Virus titers and cell infection dynamics in three parallel bioreactors for influenza A virus production. Total virus titer based on hemagglutination activity (a), infectious virus titer based on TCID₅₀ assay (b), percentage of infected (c), and apoptotic (d) MDCK cells. STR1 (■), STR2 (●), STR3 (▲)

To identify the optimal time point for virus harvest, the ratio of virus product (linear HA assay) to the total protein and the ratio of virus product to the host cell DNA concentration were determined (Figures 5b and 5d). For all STR replicates, maximum ratios were found at 21–24 hpi with 80–100 HAU/(µg_{prot}/ml) and 3–4 HAU/(ng_{DNA}/ml), respectively (Figures 5b and 5d). For both time points, the aHA titer ($3.60 \pm 0.06 \log_{10}(\text{HAU}/100 \mu\text{L})$) almost reached its plateau, but the ratio of virus product to the corresponding impurity decreased rapidly starting 24 hpi. It cannot be excluded that the further increase in aHA value (>24 hpi) does not reflect the release of virions but the accumulation of HA-containing cell debris. This is also supported by the fact that cell viability remained stable at more than 95% from the time of infection up to 24 hpi, after which it dropped significantly (Figure 1). The clarified virus harvests from 21 to 24 hpi were pooled for DSP experiments and analytics.

3.5 | IAV harvest, DNA digestion, and chemical inactivation

Low speed centrifugation (800×g) followed by dead-end microfiltration (0.45 µm) were used to remove cells and cell debris. For the pooled harvests of the optimal time of harvest (21/24 hpi) minimal

amount of cell debris after centrifugation eased the subsequent filtration step (no membrane blockage). No significant losses of aHA titers were observed for the clarified harvest material (Table 1). The DNA concentration of the clarified virus harvest was 1.2 µg/ml (Table 1). The DNA levels in the supernatant were lower when the DNA digestion was performed before the chemical inactivation by BPL (see Online Supporting Information). The host cell DNA and protein concentrations in the digested inactivated clarified virus harvest were around 28 ng/ml and 30 µg/ml, respectively (Table 1).

3.6 | Chromatographic purification of virus particles

A representative chromatogram of SXC purification step is shown in Figure 6a. Impurities such as host cell DNA and proteins were washed away in the flow-through and monitored by UV absorbance. The IAV particles were traced by light scattering, with a nil signal in the flow-through and a clear peak during elution. There was no aHA titer detected in the flow-through (Table 1), confirming the light scattering signal monitored during the chromatography run. Offline analysis of the eluate showed that the virus recovery for the SXC step was $115.2\% \pm 10.2$ and 108.0% according to the aHA and SRID

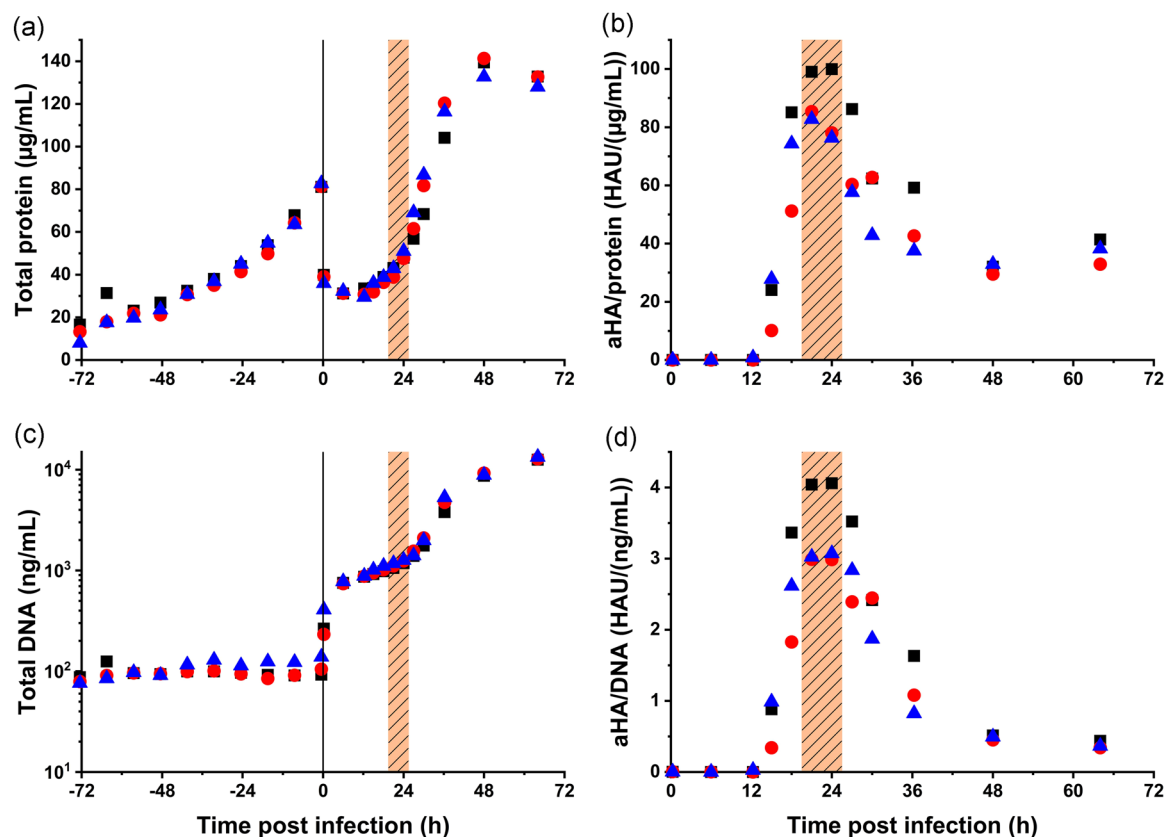


FIGURE 5 Total protein and host cell DNA profiles in three parallel bioreactors for IAV production.

Total protein (a) and total DNA (c) concentrations during the cultivation process. The ratio of total protein (b) and DNA (d) to the virus titer (aHA assay) was used to identify the optimal virus harvest point (shaded area). Vertical lines indicate the time point of infection. STR1 (■), STR2 (●), STR3 (▲). IAV, influenza A virus; HAU, hemagglutination unit

TABLE 1 Mass balances and percentile yields from the chromatographic purification of influenza A virus particles produced in 1 L STRs by capture with SXC and polishing by pseudo-affinity chromatography with a SCMA

Step	Vol. (ml)	Virus product		HA antigen ^b		Impurities		Host cell DNA ^d	
		aHA ^a	%	$\mu\text{g/mL}$	%	Total protein ^c	%	ng/mL	%
		HAU/100 μL				$\mu\text{g/mL}$			
Harvest (21 + 24 hpi) ^e		3896.1 ± 104.6	n.d.	n.d.		45.2 ± 3.6	n.d.	1171.2 ± 58.6	n.d.
Clarification (0.45 μm)		3536.4 ± 141.2	n.d.	n.d.		38.9 ± 1.2	n.d.	974.1 ± 11.8	n.d.
Digestion + inactivation ^f	50.0	1576.5 ± 105.3	n.d.	4.4		29.5 ± 2.9	n.d.	27.8 ± 2.2	n.d.
SXC load	73.6	1070.8 ± 71.6	100.0	2.9	100.0	22.7 ± 0.1	100.0	12.7 ± 0.7	100.0
SXC elution	25.0	3633.5 ± 209.9	115.2 ± 10.2	9.3	108.0	39.1 ± 0.1	58.4 ± 0.4	7.7 ± 0.7	20.6 ± 2.2
SCMA load	104.6	568.5 ± 104.6	100.0	1.8	100.0	7.8 ± 0.0	100.0	1.5 ± 0.1	100.0
SCMA elution	8.9	5584.4 ± 115.4	83.6 ± 15.5	11.8	56.0	45.3 ± 0.3	49.3 ± 0.4	7.9 ± 0.7	43.6 ± 5.5

Note: Data shown are means \pm standard deviation of the mean.

Abbreviations: dsDNA, double-stranded DNA; HAU, hemagglutination units; hpi, hours postinfection; SCMA, sulfated cellulose membrane adsorbers; STRs, stirred tank bioreactors; SXC, steric exclusion chromatography.

^aBy hemagglutination activity (aHA) assay.

^bBy single radial immunodiffusion (SRID) assay.

^cTotal protein by Bradford assay.

^ddsDNA by PicoGreen assay 40.5.

^eCentrifuged at 800 \times g.

^fEnzymatic DNA digestion followed by chemical inactivation with β -propiolactone.

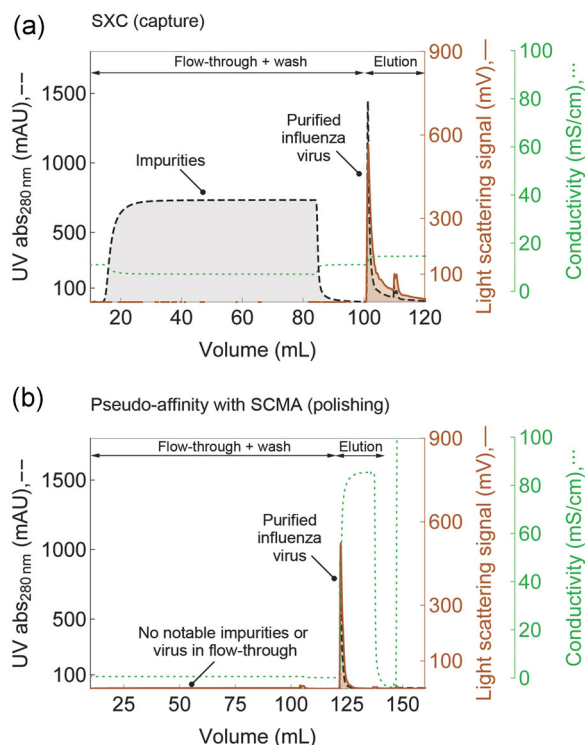


FIGURE 6 Chromatographic purification of IAV particles produced in 1 L STRs. Virus capture by SXC (a) using a column packed with regenerated cellulose membranes (100 cm²). After SXC, a polishing step was performed by pseudo affinity chromatography with an SCMA of 50 cm² (b). Virus particles were traced online by light scattering and total protein by UV absorbance. For mass balances and percentage recoveries refer to Table 1. IAV, influenza A virus; SCMA, sulfated cellulose membrane adsorbers; STRs, stirred tank bioreactors; SXC, steric exclusion chromatography

assays, respectively. The SXC eluate contained $58.4\% \pm 0.4$ of the total protein and $20.6\% \pm 2.2$ of the DNA loaded (Table 1). The eluate volume was 25 ml and was concentrated around threefold relative to the load (73.6 ml). After SXC, a pseudo-affinity chromatography polishing step was performed using an SCMA. Similar to IEX, SCMA chromatography requires low conductivity for product loading. Therefore, the SXC eluate was diluted around fourfold with SCMA binding buffer to a conductivity of 4 mS/cm. As shown in the SCMA chromatogram in Figure 6b, the UV and light-scattering signals in the flow-through were practically nil, suggesting the high purity of the loaded product and the capture of virus particles. After a washing step, the IAV particles were eluted with a high salt buffer. The product recovery in the SCMA eluate was $83.6\% \pm 15.5$ and 56.0% according to the aHA and SRID assay, respectively. The eluate contained $49.3\% \pm 0.4$ of the total protein and $43.6\% \pm 5.5$ of the DNA loaded (Table 1) and was concentrated around 10-fold (8.9 ml) relative to the load (104.6 ml).

The purified SXC eluate showed a single peak in SEC at the retention time of around 7.5 ml with no notable impurities, compared to

the SEC fingerprints of the inactivated clarified virus harvest before purification (Figure 7a). TEM pictures of the purified virus (inset) showed particles with spherical shape and a size of 80–100 nm. Purity was also confirmed by size distribution analysis of the virus particles by DCS (Figure 7b) in comparison to a process established previously (Marichal-Gallardo et al., 2017). Both the inactivated virus harvest and the purified virus samples from this study showed a monodisperse peak at around 80 nm with a few virus dimers that were slightly more notable in the purified product. Compared to the particle size distributions of the previous process, far less submicron-sized particles are observed (Figure 7b). This was probably due to the earlier harvest time of 21–24 hpi chosen for this process, compared with 72 hpi used previously (Marichal-Gallardo et al., 2017).

4 | DISCUSSION

4.1 | Cell growth and metabolism

For high yield cell culture-based vaccine manufacturing processes, high specific cell growth rates, viability, and cell concentrations are fundamental. Neglecting any of these aspects will result in compromises regarding productivity, scalability, robustness, and costs of a large-scale manufacturing process. This was also highlighted for MDCK suspension cell-based processes reported previously (Castro et al., 2015; Chu et al., 2009; Lohr et al., 2010; van Wielink et al., 2011). With an MDCK cell line exceeding 10×10^6 cells/ml that grows as single-cell suspension in a chemically defined medium with a doubling time of 21 h at viability over 97% in STR systems, a big step towards a highly competitive process is taken. Additionally, the growth performance of MDCK cells cultivated in Xeno-CDM medium was very reproducible, which eases scale-up and reduces batch-to-batch variations in USP. The established process strategy not only displayed an excellent growth performance of the cell line, but also demonstrated optimal utilization of substrates and amino acids. Whereas glucose was available in access over the whole process, glutamine and other amino acids were almost depleted towards the end of the cultivation phase and were restored partly by the fresh medium feed at time of infection. Despite a relatively strong lactate accumulation (maximal 42 mM) there was no or only a minor impact on pH and medium osmolality. A high initial glutamine concentration (>8 mM) and high specific consumption rates (30–40 fmol/(h cell)) led to ammonium concentrations of 4–5 mM both for cell growth and infection phase. For process intensification, the use of a feeding strategy using an adapted medium formulation could help to avoid volume expansion and allow to increase virus titers while reducing lactate and ammonium accumulation (Gagnon et al., 2011; Ljunggren & Häggström, 1994; Maranga & Goochee, 2006). Alternatively, glutamine and glucose could be replaced with substrates that can reduce the production of by-products (Altamirano et al., 2000; Christie & Butler, 1999; Freund & Croughan, 2018; Genzel

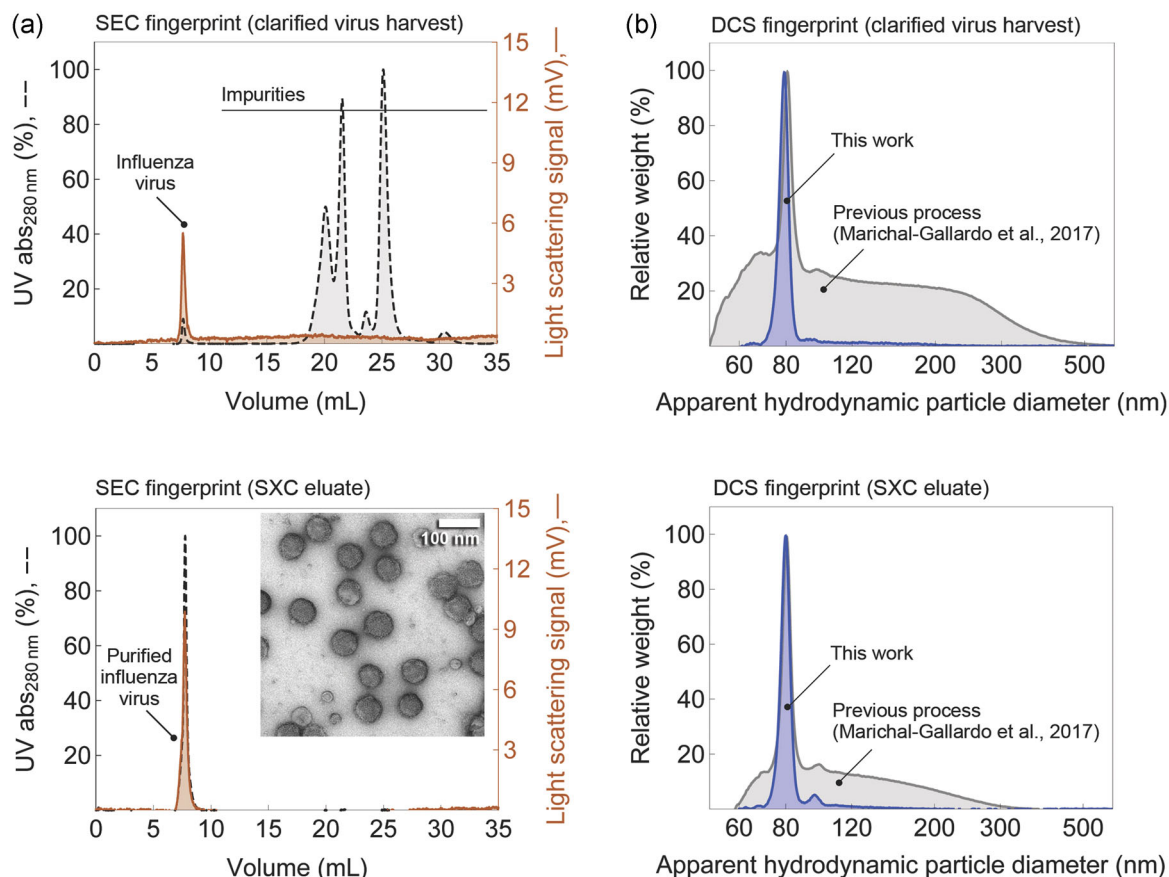


FIGURE 7 SEC fingerprints and DCS fingerprints of inactivated, clarified IAV harvests and SXC eluates. (a) The inset in the lower panel is a TEM picture of the purified virus particles. (b) For comparison of particle size distributions by DCS, samples from this study (blue curves) are shown in an overlay with samples from a similar process described previously (gray curves). DCS, differential centrifugal sedimentation; IAV, influenza A virus; SEC, size exclusion chromatography; SXC, steric exclusion chromatography; TEM, transmission electron microscopy

et al., 2005). Nevertheless, in the established process, we see no clear indication for inhibition of cell growth or virus replication due to lactate or ammonium accumulation.

4.2 | Influenza virus production

With the application of a new cultivation medium designed for MDCK suspension cells, very high IAV titers were achieved. High cell concentrations, combined with high cell-specific productivity ($>11,000$ total virions/cell; $300 \text{ TCID}_{50}/\text{cell}$) allowed to reach IAV titers that are among the highest reported for batch- or extended batch processes, and the highest titers obtained in STR systems with chemically defined media (Bissinger et al., 2019; Bock et al., 2011; Hu et al., 2011; Huang et al., 2015; Le Ru et al., 2010; Peschel et al., 2013). Furthermore, high cell growth and fast virus replication reduced the USP production time from 7 to 4 days, compared with adherent MDCK cells (Genzel, Fischer, et al., 2006; Genzel, Olmer, et al., 2006; Hu et al., 2008). In combination with the achieved virus titers ($3.6 \log_{10}(\text{HAU}/100 \mu\text{l})$ and $>2 \times 10^9 \text{ TCID}_{50}/\text{ml}$) this increases overall productivity, and can support fast manufacturing of pandemic vaccines.

4.3 | Transition from USP to DSP

One of the most important aspects regarding process intensification in USP is the control of protein and host cell DNA contamination levels in the DSP train. Challenges arise if the time point of harvest is not selected properly and IAV-induced cell lysis results in an unnecessary high release of contaminants. Consequently, it might be required to increase the number of DSP unit operations with a negative impact on process yield and cost effectiveness. For instance, the clearance of cellular chromatin—one of the most persistent process impurities—is challenging even for affinity-based purification methods. Therefore, it is desirable to harvest the product in a time window where titers peak but cell lysis is not too advanced (Gagnon et al., 2014, 2015; Nian & Gagnon, 2016; Tan et al., 2015). Here, we identified the optimal harvest point based on the highest ratio of virus titer to total protein (Figure 5b) and host cell DNA (Figure 5d) to minimize the amount of impurities for subsequent DSP steps. For each of the three STRs, the best ratio of virus product to impurities was in a time window of 21–24 hpi and therefore, harvests were pooled for DSP (see Figure 5). The slightly higher product to impurity ratio of STR number 1 compared with STRs number 2 and 3 was most likely attributed to normal batch-to-batch variation.

The placement of the enzymatic DNA digestion step in the process was an additional factor to be considered for reduction of the amount of host cell DNA before the chromatography. Two options were tested: placing the nuclease treatment either before or immediately after the chemical inactivation of IAV with BPL. The DNA concentration was reduced more than threefold by performing the nuclease digestion step before the BPL treatment (Table S1). BPL-induced cross-linking reactions between nucleic acid and proteins might explain higher residual DNA in case inactivation is performed first, as the DNase might not be able to digest the chemically modified DNA (Kubinski & Szybalski, 1975). Depending on the process train, BPL inactivation of the purified product might allow to further reduce the level of host cell DNA as reported previously (Gegersen et al., 2011).

4.4 | Virus purification

Membrane-based SXC was used successfully as a capture step with virtually full product recovery for both the total IAV content (aHA assay) and the HA antigen content (SRID assay) as previously reported for a similar process (Marichal-Gallardo et al., 2017). Compared to other chromatography techniques for purification of IAV and other viruses, SXC appears to be comparable or better in terms of product recovery and ease of use, as also discussed previously (Marichal-Gallardo et al., 2017, 2021). The ability to load and recover the product at physiological salt concentration and pH value minimizes the risk of losing biological activity compared with other techniques. Additionally to the virus strain used in this study (A/Puerto Rico/8/34 H1N1), different influenza virus strains (A/Switzerland/9715293/2013 H3N2, B/Phuket/3073/2013 (Yamagata), and B/Brisbane/63/2014 (Victoria)) have been purified with SXC using the same process conditions,

rendering SXC a promising and efficient platform technology for cell culture-based influenza vaccine manufacturing (Marichal-Gallardo, 2019). In this study, most of the host cell DNA was cleared by the nuclease treatment before SXC. The SXC step additionally cleared about 80% of DNA and about 40% of total protein. Interestingly, the subsequent polishing step using an SCMA did not further improve the purity of the virus particles (Table 1), evidencing the importance of carefully selecting the harvesting time point and the order of the unit operations.

Considering a monovalent vaccine dose of 15 μg_{HA} (SRID assay), Table 2 shows that the SXC and SCMA eluates are either below the accepted contamination levels for protein (<100 μg per strain per dose) or close to the maximum of 10 ng of DNA per dose accepted. However, according to Ikeda et al. (2009), and based on our experience, the DNA concentrations measured with the PicoGreen assay (as short as 20 bp) are about 5–10 times higher than those detected with the Threshold assay that quantifies fragments larger than 100 bp and is often used for product release (Marichal-Gallardo et al., 2017; Weigel et al., 2016). Assuming a ratio of five would hypothetically result in a residual DNA contamination level of around 2 ng per monovalent dose. As PicoGreen quantification also detects RNA (with about 100 times lower sensitivity), the actual DNA level in the final product could be even lower (Singer et al., 1997). Eventually, the evaluation of the performance of the process established will depend on the specific assay validated for product release.

Here, the combination of both chromatography methods resulted in a cumulative product recovery of around 96% by aHA assay and 60% by SRID assay. This would be equivalent to about 170 doses/L (5.9 ml/dose) of virus harvest. In case only SXC is used, about 300 doses/L (3.3 ml/dose) of virus harvest were estimated. Regarding overall losses of the entire DSP train, improvements can be made primarily in the initial clarification, viral inactivation, and DNA

Step	aHA ^a Yield (%)	HA antigen ^b Yield (%)	Purified doses ^c per L of harvest	Protein per dose (μg) ^d	DNA per dose (ng) ^e
SXC	115.2 \pm 10.2	108.0	309	63.3 \pm 0.2	12.5 \pm 1.1
SCMA	83.6 \pm 15.5	56.0	173	57.5 \pm 0.3	10.0 \pm 0.9
Σ^f	96.3 \pm 1.6	60.4			

Note: Data shown are means \pm standard deviation of the mean.

Abbreviations: dsDNA, double-stranded DNA; SCMA, sulfated cellulose membrane adsorbers; SXC, steric exclusion chromatography.

^aBy hemagglutination activity (aHA) assay.

^bBy single radial immunodiffusion (SRID) assay.

^cMonovalent dose of 15 μg_{HA} .

^dTotal protein by Bradford assay; <6 \times HA antigen content and <100 μg per strain total protein per dose.

^edsDNA by PicoGreen assay; max. 10 ng per dose.

^fCumulative yield.

TABLE 2 Estimated number of influenza vaccine doses (15 μg_{HA} per dose) after purification with SXC and SCMA

digestion steps before the SXC capture step (Table 1). Finally, as the process suggested here is to produce whole virus particles, additional DSP steps might be required for formulation of split or subunit vaccines that most likely allow purity improvements (Bron et al., 1993; Cusi, 2006).

Either SXC only or a combination of SXC and SCMA is possible for IAV purification. Both methods can be easily integrated, and can be operated at much higher flow rates compared to packed beds using beads because they have no diffusional limitations. In addition, scale-up of SXC and SCMA is linear by simply increasing the membrane surface. Furthermore, both methods are single-use which reduces capital and operational costs, facility downtimes, contamination risks, and avoid validation of cleaning and sanitization procedures.

4.5 | Overall process performance

For vaccine production, not only individual process steps but options for scale-up and process integration are crucial. Based on the growth properties of the MDCK suspension cell line developed here, we assume a reduced lead time to reach manufacturing scale (i.e., 2,000 or 10,000 L), compared to other cell lines with a higher cell doubling time and a lower maximal cell density (e.g., t_D 30 h; VCC 5×10^6 cells/ml). Furthermore, the established production process is shorter and more productive than other processes using MDCK suspension cell lines (Huang et al., 2015; Lohr et al., 2010; Wang et al., 2017). Scale-up from shaker flasks to lab-scale bioreactors showed no significant changes in terms of cell concentration, cell viability, and virus product produced (Table S2) and we don't expect major scalability issues moving to larger scales.

The most significant losses during DSP were observed in the viral inactivation and DNA digestion steps, which presents an opportunity for improvement to increase the number of purified doses obtained. With the assumption of a fixed aHA to HA protein ratio (400 in this case) an HA antigen content of roughly 9 µg/ml was estimated for the clarified harvest which would correlate to a potential USP production capacity of approximately 600 doses/L. The polishing step by SCMA improved purity only marginally at the expense of additional product losses. However, the pseudo-affinity step with SCMA provides an orthogonal purification method for several influenza strains that can further concentrate the product and eliminate traces of PEG from the SXC eluates (Fortuna et al., 2019). Ultimately, the inability of the SCMA step to drastically improve purity under the conditions tested here, evidence the high quality of the produced SXC eluate (Figure 7). Alternative to SCMA, other purification methods such as anion exchange chromatography, cross-flow filtration, or virion splitting might further improve the purity of the SXC product.

Overall, the productivity of up to 300 purified vaccine doses (15 µg/dose) per liter of cultivation in 4–5 days was determined. This represents the potential for producing three million vaccine doses at the 10,000 L scale. As a comparison, an egg-based influenza vaccine process that typically yields one dose per egg (Buckland, 2015), takes

around three weeks to test the growth conditions of a virus candidate while producing each batch of antigen takes approximately two weeks (World Health Organization, 2009).

From small-scale purification experiments with the membrane-based chromatography, we estimated productivity as high as 4600 doses/(m² h) (15 µg/dose). Both SXC and SCMA can be operated at industrial scales with devices similar to ones already available for other chromatography techniques such as IEX with a surface area of 18 m². For SXC, 83,000 doses/h could be purified with such a device. Concerning the resulting quality of the vaccine candidate, we were only able to assess structural integrity and purity. Additional animal trials would be necessary as the next step towards a commercial product. With this the effective vaccine dose can be determined in clinical follow-up studies and additional critical process parameters concerning product quality could be identified.

This study describes a promising manufacturing platform with many advantages and higher productivity compared to egg-based influenza vaccine processes. Albeit room for improvement, our reported process has the potential to be implemented with minor modifications (e.g., for different influenza strains) for the quick manufacturing of large quantities of influenza vaccines, thus significantly improving pandemic preparedness and response.

ACKNOWLEDGMENTS

The authors would like to thank Claudia Best, Nancy Wynserski, Lisa Fichtmüller, and Anja Bastian for their excellent technical support. The authors greatly appreciate the contribution of Shanghai BioEngine Sci-Tech by providing the Xeno-CDM medium. Yixiao Wu acknowledges the financial support of the China Scholarship Council. Pavel Marichal-Gallardo acknowledges the financial support of of Consejo Nacional de Ciencia y Tecnología (CONACYT Mexico; grant 455827-399845). Open access funding enabled and organized by Projekt DEAL.

CONFLICT OF INTERESTS

Wen-Song Tan and Xuping Liu are affiliated as directors with Shanghai BioEngine Sci-Tech and were involved in the development of the Xeno-CDM medium both for scientific and commercial purposes. Pavel Marichal-Gallardo and Udo Reichl are inventors on pending patent applications related to the SXC purification method described in this study. Udo Reichl is an inventor on granted patents related to the SCMA purification method described in this study. The remaining authors declare that they have no conflict of interests.

DATA AVAILABILITY STATEMENT

The data that support the findings of this study are available from the corresponding author upon reasonable request.

ORCID

Thomas Bissinger  <http://orcid.org/0000-0002-6901-6161>

Yixiao Wu  <http://orcid.org/0000-0002-3616-3026>

Pavel Marichal-Gallardo  <http://orcid.org/0000-0002-5540-4454>

Yvonne Genzel  <http://orcid.org/0000-0002-2652-5943>

Wen-Song Tan  <http://orcid.org/0000-0001-9857-4798>

Udo Reichl  <http://orcid.org/0000-0001-6538-1332>

REFERENCES

- Aggarwal, K., Jing, F., Maranga, L., & Liu, J. (2011). Bioprocess optimization for cell culture based influenza vaccine production. *Vaccine*, 29(17), 3320–3328. <https://doi.org/10.1016/j.vaccine.2011.01.081>
- Altamirano, C., Paredes, C., Cairó, J. J., & Gòdia, F. (2000). Improvement of CHO cell culture medium formulation: Simultaneous substitution of glucose and glutamine. *Biotechnology Progress*, 16(1), 69–75. <https://doi.org/10.1021/bp990124j>
- Audsley, J. M., & Tannock, G. A. (2004). The role of cell culture vaccines in the control of the next influenza pandemic. *Expert Opinion on Biological Therapy*, 4(5), 709–717. <https://doi.org/10.1517/14712598.4.5.709>
- B Carvalho, S., Fortuna, A. R., Wolff, M. W., Peixoto, C., M Alves, P., Reichl, U., & JT Carrondo, M. (2018). Purification of influenza virus-like particles using sulfated cellulose membrane adsorbers. *Journal of Chemical Technology & Biotechnology*, 93(7), 1988–1996. <https://doi.org/10.1002/jctb.5474>
- Baek, J.-O., Seo, J.-W., Kim, I.-H., & Kim, C. H. (2011). Production and purification of human papillomavirus type 33 L1 virus-like particles from Spodoptera frugiperda 9 cells using two-step column chromatography. *Protein Expression and Purification*, 75(2), 211–217. <https://doi.org/10.1016/j.pep.2010.08.005>
- Barr, I. G., Donis, R. O., Katz, J. M., McCauley, J. W., Odagiri, T., Trusheim, H., Tsai, T. F., & Wentworth, D. E. (2018). Cell culture-derived influenza vaccines in the severe 2017–2018 epidemic season: A step towards improved influenza vaccine effectiveness. *NPJ Vaccines*, 3, 44. <https://doi.org/10.1038/s41541-018-0079-z>
- Bissinger, T., Fritsch, J., Mihut, A., Wu, Y., Liu, X., Genzel, Y., Tan, W. S., & Reichl, U. (2019). Semi-perfusion cultures of suspension MDCK cells enable high cell concentrations and efficient influenza A virus production. *Vaccine*, 37, 7003–7010. <https://doi.org/10.1016/j.vaccine.2019.04.054>
- Bock, A., Schulze-Horsel, J., Schwarzer, J., Rapp, E., Genzel, Y., & Reichl, U. (2011). High-density microcarrier cell cultures for influenza virus production. *Biotechnology Progress*, 27(1), 241–250. <https://doi.org/10.1002/btpr.539>
- Bresee, J. S., Fry, A. M., Sambhara, S., & Cox, N. J. (2018). 31-inactivated influenza vaccines. In S. A. Plotkin, W. A. Orenstein, P. A. Offit, & K. M. Edwards (Eds.), *Plotkin's vaccines* (7th ed., pp. 456–488). Elsevier.
- Bron, R., Ortiz, A., Dijkstra, J., Stegmann, T., & Wilschut, J. (1993). Preparation, properties, and applications of reconstituted influenza virus envelopes (viroosomes). *Methods in Enzymology*, 220, 313–331.
- Buckland, B. C. (2015). The development and manufacture of influenza vaccines. *Human Vaccines & Immunotherapeutics*, 11(6), 1357–1360. <https://doi.org/10.1080/21645515.2015.1026497>
- Castro, R., Fernandes, P., Laske, T., Sousa, M. F., Genzel, Y., Scharfenberg, K., Alves, P. M., & Coroadinha, A. S. (2015). Production of canine adenovirus type 2 in serum-free suspension cultures of MDCK cells. *Applied Microbiology and Biotechnology*, 99(17), 7059–7068. <https://doi.org/10.1007/s00253-015-6636-8>
- Centers for Disease Control and Prevention. (2020). *Clinical update announcement: Temporary total depletion of US licensed yellow fever vaccine addressed by availability of stamril vaccine at selected clinics*. <https://wwwnc.cdc.gov/travel/news-announcements/yellow-fever-vaccine-access>
- Christie, A., & Butler, M. (1999). The adaptation of bhk cells to a non-ammonia-glutamate-based culture medium. *Biotechnology and Bioengineering*, 64(3), 298–309. [https://doi.org/10.1002/\(sici\)1097-0290\(19990805\)64:3%3C298::Aid-bit6%3E3.0.Co;2-u](https://doi.org/10.1002/(sici)1097-0290(19990805)64:3%3C298::Aid-bit6%3E3.0.Co;2-u)
- Chu, C., Lugovtsev, V., Golding, H., Betenbaugh, M., & Shiloach, J. (2009). Conversion of MDCK cell line to suspension culture by transfecting with human *siat7e* gene and its application for influenza virus production. *Proceedings of the National Academy of Sciences of the United States of America*, 106(35), 14802–14807. <https://doi.org/10.1073/pnas.0905912106>
- Coronel, J., Behrendt, I., Bürgin, T., Anderlei, T., Sandig, V., Reichl, U., & Genzel, Y. (2019). Influenza A virus production in a single-use orbital shaken bioreactor with ATF or TFF perfusion systems. *Vaccine*, 37, 7011–7018. <https://doi.org/10.1016/j.vaccine.2019.06.005>
- Cusi, M. G. (2006). Applications of influenza viroosomes as a delivery system. *Human Vaccines*, 2(1), 1–7. <https://doi.org/10.4161/hv.2.1.2494>
- Doroshenko, A., & Halperin, S. A. (2009). Trivalent MDCK cell culture-derived influenza vaccine Optaflu® (Novartis Vaccines). *Expert Review of Vaccines*, 8(6), 679–688. <https://doi.org/10.1586/erv.09.31>
- Dukes, J. D., Whitley, P., & Chalmers, A. D. (2011). The MDCK variety pack: Choosing the right strain. *BMC Cell Biology*, 12(1), 43. <https://doi.org/10.1186/1471-2121-12-43>
- Eagle, H. (1959). Amino acid metabolism in mammalian cell cultures. *Science*, 130(3373), 432–437. <https://doi.org/10.1126/science.130.3373.432>
- Ernest, M., & Kamen, A. A. (2015). Current and emerging cell culture manufacturing technologies for influenza vaccines. *BioMed Research International*, 2015, 11. <https://doi.org/10.1155/2015/504831>
- Ferguson, N. M., Cummings, D. A. T., Fraser, C., Cajka, J. C., Cooley, P. C., & Burke, D. S. (2006). Strategies for mitigating an influenza pandemic. *Nature*, 442, 448–452. <https://doi.org/10.1038/nature04795>
- Fineberg, H. V. (2014). Pandemic preparedness and response: lessons from the H1N1 influenza of 2009. *New England Journal of Medicine*, 370(14), 1335–1342. <https://doi.org/10.1056/NEJMr1208802>
- Fortuna, A. R., Taft, F., Villain, L., Wolff, M. W., & Reichl, U. (2018). Optimization of cell culture-derived influenza A virus particles purification using sulfated cellulose membrane adsorbers. *Engineering in Life Sciences*, 18(1), 29–39. <https://doi.org/10.1002/elsc.201700108>
- Fortuna, A. R., van Teeffelen, S., Ley, A., Fischer, L. M., Taft, F., Genzel, Y., Villain, L., Wolff, M. W., & Reichl, U. (2019). Use of sulfated cellulose membrane adsorbers for chromatographic purification of cell cultured-derived influenza A and B viruses. *Separation and Purification Technology*, 226, 350–358. <https://doi.org/10.1016/j.seppur.2019.05.101>
- Frensing, T., Kupke, S. Y., Bachmann, M., Fritzsche, S., Gallo-Ramirez, L. E., & Reichl, U. (2016). Influenza virus intracellular replication dynamics, release kinetics, and particle morphology during propagation in MDCK cells. *Applied Microbiology and Biotechnology*, 100(16), 7181–7192. <https://doi.org/10.1007/s00253-016-7542-4>
- Freund, N. W., & Croughan, M. S. (2018). A simple method to reduce both lactic acid and ammonium production in industrial animal cell culture. *International Journal of Molecular Sciences*, 19(2), 385.
- Gagnon, M., Hiller, G., Luan, Y.-T., Kittredge, A., DeFelice, J., & Drapeau, D. (2011). High-end pH-controlled delivery of glucose effectively suppresses lactate accumulation in CHO Fed-batch cultures. *Biotechnology and Bioengineering*, 108(6), 1328–1337. <https://doi.org/10.1002/bit.23072>
- Gagnon, P. (2010). Chromatographic purification of virus particles. In M. C. Flickinger (Ed.), *Encyclopedia of industrial biotechnology* (pp. 415–436). John Wiley & Sons, Inc.
- Gagnon, P., Nian, R., Tan, L., Cheong, J., Yeo, V., Yang, Y., & Gan, H. T. (2014). Chromatin-mediated depression of fractionation performance on electronegative multimodal chromatography

- media, its prevention, and ramifications for purification of immunoglobulin G. *Journal of Chromatography A*, 1374, 145–155. <https://doi.org/10.1016/j.chroma.2014.11.052>
- Gagnon, P., Nian, R., Yang, Y., Yang, Q., & Lim, C. L. (2015). Non-immunospecific association of immunoglobulin G with chromatin during elution from protein A inflates host contamination, aggregate content, and antibody loss. *Journal of Chromatography A*, 1408, 151–160. <https://doi.org/10.1016/j.chroma.2015.07.017>
- Gallo-Ramirez, L. E., Nikolay, A., Genzel, Y., & Reichl, U. (2015). Bioreactor concepts for cell culture-based viral vaccine production. *Expert Review of Vaccines*, 14(9), 1181–1195. <https://doi.org/10.1586/14760584.2015.1067144>
- Genzel, Y., Fischer, M., & Reichl, U. (2006). Serum-free influenza virus production avoiding washing steps and medium exchange in large-scale microcarrier culture. *Vaccine*, 24(16), 3261–3272. <https://doi.org/10.1016/j.vaccine.2006.01.019>
- Genzel, Y., Olmer, R. M., Schäfer, B., & Reichl, U. (2006). Wave microcarrier cultivation of MDCK cells for influenza virus production in serum containing and serum-free media. *Vaccine*, 24(35), 6074–6087. <https://doi.org/10.1016/j.vaccine.2006.05.023>
- Genzel, Y., & Reichl, U. (2007). Vaccine production. In R. Pörtner (Ed.), *Animal cell biotechnology: Methods and protocols* (pp. 457–473). Humana Press.
- Genzel, Y., & Reichl, U. (2009). Continuous cell lines as a production system for influenza vaccines. *Expert Review of Vaccines*, 8(12), 1681–1692. <https://doi.org/10.1586/erv.09.128>
- Genzel, Y., Ritter, J. B., König, S., Alt, R., & Reichl, U. (2005). Substitution of glutamine by pyruvate to reduce ammonia formation and growth inhibition of mammalian cells. *Biotechnology Progress*, 21(1), 58–69. <https://doi.org/10.1021/bp049827d>
- George, M., Farooq, M., Dang, T., Cortes, B., Liu, J., & Maranga, L. (2010). Production of cell culture (MDCK) derived live attenuated influenza vaccine (LAIV) in a fully disposable platform process. *Biotechnology and Bioengineering*, 106(6), 906–917. <https://doi.org/10.1002/bit.22753>
- Girard, M. P., Tam, J. S., Assossou, O. M., & Kiény, M. P. (2010). The 2009 A (H1N1) influenza virus pandemic: A review. *Vaccine*, 28(31), 4895–4902. <https://doi.org/10.1016/j.vaccine.2010.05.031>
- Gregersen, J.-P., Schmitt, H.-J., Trusheim, H., & Bröker, M. (2011). Safety of MDCK cell culture-based influenza vaccines. *Future Microbiology*, 6(2), 143–152. <https://doi.org/10.2217/fmb.10.161>
- Horimoto, T., & Kawaoka, Y. (2001). Pandemic threat posed by avian influenza A viruses. *Clinical Microbiology Reviews*, 14(1), 129–149. <https://doi.org/10.1128/cmr.14.1.129-149.2001>
- Hu, A., Weng, T.-C., Tseng, Y.-F., Chen, Y.-S., Wu, C.-H., Hsiao, S., & Lee, M.-S. (2008). Microcarrier-based MDCK cell culture system for the production of influenza H5N1 vaccines. *Vaccine*, 26(45), 5736–5740.
- Hu, A. Y., Tseng, Y.-F., Weng, T.-C., Liao, C.-C., Wu, J., Chou, A.-H., Chao, H. J., Gu, A., Chen, J., Lin, S. C., Hsiao, C. H., Wu, S. C., & Chong, P. (2011). Production of inactivated influenza H5N1 vaccines from MDCK cells in serum-free medium. *PLoS One*, 6(1), e14578. <https://doi.org/10.1371/journal.pone.0014578>
- Huang, D., Peng, W. J., Ye, Q., Liu, X. P., Zhao, L., Fan, L., Xia-Hou, K., Jia, H. J., Luo, J., Zhou, L. T., Li, B. B., Wang, S. L., Xu, W. T., Chen, Z., & Tan, W. S. (2015). Serum-free suspension culture of MDCK cells for production of influenza H1N1 vaccines. *PLoS One*, 10(11), e0141686. <https://doi.org/10.1371/journal.pone.0141686>
- Huang, D., Zhao, L., & Tan, W. (2011). Adherent and single-cell suspension culture of Madin-Darby canine kidney cells in serum-free medium. *Sheng wu Gong Cheng xue Bao = Chinese Journal of Biotechnology*, 27(4), 645–652.
- Ikeda, Y., Iwakiri, S., & Yoshimori, T. (2009). Development and characterization of a novel host cell DNA assay using ultra-sensitive fluorescent nucleic acid stain "PicoGreen". *Journal of Pharmaceutical and Biomedical Analysis*, 49(4), 997–1002. <https://doi.org/10.1016/j.jpba.2009.01.022>
- Jin, H., & Subbarao, K. (2015). Live attenuated influenza vaccine. In M. B. A. Oldstone, & R. W. Compans (Eds.), *Influenza pathogenesis and control* (Vol. II, pp. 181–204). Springer International Publishing.
- Kalbfuss, B., Knochlein, A., Krober, T., & Reichl, U. (2008). Monitoring influenza virus content in vaccine production: Precise assays for the quantitation of hemagglutination and neuraminidase activity. *Biologicals*, 36(3), 145–161. <https://doi.org/10.1016/j.biologicals.2007.10.002>
- Kärber, G. (1931). Beitrag zur kollektiven behandlung pharmakologischer reihenversuche. *Naunyn-Schmiedebergs Archiv für Experimentelle Pathologie und Pharmakologie*, 162(4), 480–483. <https://doi.org/10.1007/bf01863914>
- Kilbourne, E. D. (2006). Influenza pandemics of the 20th century. *Emerging Infectious Diseases*, 12(1), 9–14. <https://doi.org/10.3201/eid1201.051254>
- Kostova, D., Reed, C., Finelli, L., Cheng, P.-Y., Gargiullo, P. M., Shay, D. K., Singleton, J. A., Meltzer, M. I., Lu, P. J., & Bresee, J. S. (2013). Influenza illness and hospitalizations averted by influenza vaccination in the United States, 2005–2011. *PLoS One*, 8(6), e66312. <https://doi.org/10.1371/journal.pone.0066312>
- Kröber, T., Wolff, M. W., Hundt, B., Seidel-Morgenstern, A., & Reichl, U. (2013). Continuous purification of influenza virus using simulated moving bed chromatography. *Journal of Chromatography A*, 1307, 99–110. <https://doi.org/10.1016/j.chroma.2013.07.081>
- Kubinski, H., & Szybalski, E. H. (1975). Intermolecular linking and fragmentation of DNA by β -propiolactone, a monoalkylating carcinogen. *Chemico-Biological Interactions*, 10(1), 41–55. [https://doi.org/10.1016/0009-2797\(75\)90045-9](https://doi.org/10.1016/0009-2797(75)90045-9)
- Kuiper, M., Sanches, R. M., Walford, J. A., & Slater, N. K. H. (2002). Purification of a functional gene therapy vector derived from Moloney murine leukaemia virus using membrane filtration and ceramic hydroxyapatite chromatography. *Biotechnology and Bioengineering*, 80(4), 445–453. <https://doi.org/10.1002/bit.10388>
- Le Ru, A., Jacob, D., Transfiguracion, J., Ansorge, S., Henry, O., & Kamen, A. A. (2010). Scalable production of influenza virus in HEK-293 cells for efficient vaccine manufacturing. *Vaccine*, 28(21), 3661–3671. <https://doi.org/10.1016/j.vaccine.2010.03.029>
- Lee, M. F. X., Chan, E. S., Tan, W. S., Tam, K. C., & Tey, B. T. (2015). Negative chromatography purification of hepatitis B virus-like particles using poly(oligo(ethylene glycol) methacrylate) grafted cationic adsorbent. *Journal of Chromatography A*, 1415, 161–165. <https://doi.org/10.1016/j.chroma.2015.08.056>
- Li, H., Yang, Y., Zhang, Y., Zhang, S., Zhao, Q., Zhu, Y., Zou, X., Yu, M., Ma, G., & Su, Z. (2015). A hydrophobic interaction chromatography strategy for purification of inactivated foot-and-mouth disease virus. *Protein Expression and Purification*, 113, 23–29. <https://doi.org/10.1016/j.pep.2015.04.011>
- Li, K. S., Guan, Y., Wang, J., Smith, G. J., Xu, K. M., Duan, L., Rahardjo, A. P., Puthavathana, P., Buranathai, C., Nguyen, T. D., Estoepongastie, A. T., Chaisingh, A., Auewarakul, P., Long, H. T., Hanh, N. T., Webby, R. J., Poon, L. L., Chen, H., Shortridge, K. F., ... Peiris, J. S. (2004). Genesis of a highly pathogenic and potentially pandemic H5N1 influenza virus in eastern Asia. *Nature*, 430, 209–213. <https://doi.org/10.1038/nature02746>
- Ljunggren, J., & Häggström, L. (1994). Catabolic control of hybridoma cells by glucose and glutamine limited fed batch cultures. *Biotechnology and Bioengineering*, 44(7), 808–818. <https://doi.org/10.1002/bit.260440706>
- Lohr, V., Genzel, Y., Behrendt, I., Scharfenberg, K., & Reichl, U. (2010). A new MDCK suspension line cultivated in a fully defined medium in stirred-tank and wave bioreactor. *Vaccine*, 28(38), 6256–6264. <https://doi.org/10.1016/j.vaccine.2010.07.004>

- Lopes, A. G. (2015). Single-use in the biopharmaceutical industry: A review of current technology impact, challenges and limitations. *Food and Bioproducts Processing*, 93, 98–114. <https://doi.org/10.1016/j.fbp.2013.12.002>
- Maranga, L., & Goochee, C. F. (2006). Metabolism of PER.C6TM cells cultivated under fed-batch conditions at low glucose and glutamine levels. *Biotechnology and Bioengineering*, 94(1), 139–150. <https://doi.org/10.1002/bit.20890>
- Marichal-Gallardo, P. (2019). *Chromatographic purification of biological macromolecules by their capture on hydrophilic surfaces with the aid of non-ionic polymers* (PhD thesis). Otto von Guericke University Magdeburg. <http://hdl.handle.net/21.11116/0000-0006-DA17-B>
- Marichal-Gallardo, P., Börner, K., Pieler, M. M., Sonntag-Buck, V., Obr, M., Bejarano, D., Wolff, M. W., Kräusslich, H. G., Reichl, U., & Grimm, D. (2021). Single-use capture purification of adeno-associated viral gene transfer vectors by membrane-based steric exclusion chromatography. *Human Gene Therapy*, <https://doi.org/10.1089/hum.2019.284>
- Marichal-Gallardo, P., Pieler, M. M., Wolff, M. W., & Reichl, U. (2017). Steric exclusion chromatography for purification of cell culture-derived influenza A virus using regenerated cellulose membranes and polyethylene glycol. *Journal of Chromatography A*, 1483, 110–119. <https://doi.org/10.1016/j.chroma.2016.12.076>
- Momose, F., Kikuchi, Y., Komase, K., & Morikawa, Y. (2007). Visualization of microtubule-mediated transport of influenza viral progeny ribonucleoprotein. *Microbes and Infection*, 9(12), 1422–1433. <https://doi.org/10.1016/j.micinf.2007.07.007>
- Montomoli, E., Khadang, B., Piccirella, S., Trombetta, C., Mennitto, E., Manini, I., Stanzani, V., & Lapini, G. (2012). Cell culture-derived influenza vaccines from Vero cells: a new horizon for vaccine production. *Expert Review of Vaccines*, 11(5), 587–594. <https://doi.org/10.1586/erv.12.24>
- Morenweiser, R. (2005). Downstream processing of viral vectors and vaccines. *Gene Therapy*, 12, S103–S110. <https://doi.org/10.1038/sj.gt.3302624>
- Nian, R., & Gagnon, P. (2016). Advance chromatin extraction enhances performance and productivity of cation exchange chromatography-based capture of Immunoglobulin G monoclonal antibodies. *Journal of Chromatography A*, 1453, 54–61. <https://doi.org/10.1016/j.chroma.2016.05.029>
- Onions, D., Egan, W., Jarrett, R., Novicki, D., & Gregersen, J.-P. (2010). Validation of the safety of MDCK cells as a substrate for the production of a cell-derived influenza vaccine. *Biologicals*, 38(5), 544–551. <https://doi.org/10.1016/j.biologicals.2010.04.003>
- Opitz, L., Lehmann, S., Reichl, U., & Wolff, M. W. (2009). Sulfated membrane adsorbers for economic pseudo-affinity capture of influenza virus particles. *Biotechnology and Bioengineering*, 103(6), 1144–1154. <https://doi.org/10.1002/bit.22345>
- Peschel, B., Frentzel, S., Laske, T., Genzel, Y., & Reichl, U. (2013). Comparison of influenza virus yields and apoptosis-induction in an adherent and a suspension MDCK cell line. *Vaccine*, 31(48), 5693–5699. <https://doi.org/10.1016/j.vaccine.2013.09.051>
- Pieler, M. M., Heyse, A., Wolff, M. W., & Reichl, U. (2017). Specific ion effects on the particle size distributions of cell culture-derived influenza A virus particles within the Hofmeister series. *Engineering in Life Sciences*, 17(5), 470–478. <https://doi.org/10.1002/elsc.201600153>
- Raymond, D. D., Stewart, S. M., Lee, J., Ferdman, J., Bajic, G., Do, K. T., Ernandes, M. J., Suphaphiphat, P., Settembre, E. C., Dormitzer, P. R., Del Giudice, G., Finco, O., Kang, T. H., Ippolito, G. C., Georgiou, G., Kepler, T. B., Haynes, B. F., Moody, M. A., Liao, H. X., ... Harrison, S. C. (2016). Influenza immunization elicits antibodies specific for an egg-adapted vaccine strain. *Nature Medicine*, 22(12), 1465–1469. <https://doi.org/10.1038/nm.4223>
- Schild, G. C., Oxford, J. S., de Jong, J. C., & Webster, R. G. (1983). Evidence for host-cell selection of influenza virus antigenic variants. *Nature*, 303(5919), 706–709. <https://doi.org/10.1038/303706a0>
- Schneider, M., Marison, I. W., & von Stockar, U. (1996). The importance of ammonia in mammalian cell culture. *Journal of Biotechnology*, 46(3), 161–185. [https://doi.org/10.1016/0168-1656\(95\)00196-4](https://doi.org/10.1016/0168-1656(95)00196-4)
- Singer, V. L., Jones, L. J., Yue, S. T., & Haugland, R. P. (1997). Characterization of PicoGreen reagent and development of a fluorescence-based solution assay for double-stranded DNA quantitation. *Analytical Biochemistry*, 249(2), 228–238. <https://doi.org/10.1006/abio.1997.2177>
- Skowronski, D. M., Janjua, N. Z., De Serres, G., Sabaiduc, S., Eshaghi, A., Dickinson, J. A., Fonseca, K., Winter, A. L., Gubbay, J. B., Kraiden, M., Petric, M., Charest, H., Bastien, N., Kwindt, T. L., Mahmud, S. M., Van Caesele, P., & Li, Y. (2014). Low 2012–13 influenza vaccine effectiveness associated with mutation in the egg-adapted H3N2 vaccine strain not antigenic drift in circulating viruses. *PLoS One*, 9(3), e92153. <https://doi.org/10.1371/journal.pone.0092153>
- Slivac, I., Blajić, V., Radošević, K., Kniewald, Z., & Gaurina Srček, V. (2010). Influence of different ammonium, lactate and glutamine concentrations on CCO cell growth. *Cytotechnology*, 62(6), 585–594. <https://doi.org/10.1007/s10616-010-9312-y>
- Sparrow, E., Wood, J. G., Chadwick, C., Newall, A. T., Torvaldsen, S., Moen, A., & Torelli, G. (2021). Global production capacity of seasonal and pandemic influenza vaccines in 2019. *Vaccine*, 39(3), 512–520. <https://doi.org/10.1016/j.vaccine.2020.12.018>
- Spearman, C. (1909). Review of the method of 'Right and Wrong Cases' ('Constant Stimuli') without Gauss's formula. *Psychological Bulletin*, 6(1), 27–28. <https://doi.org/10.1037/h0063767>
- Stöhr, K. (2014). Perspective: Ill prepared for a pandemic. *Nature*, 507(7490), S20–S21. <https://doi.org/10.1038/507S20a>
- Tan, L., Yeo, V., Yang, Y., & Gagnon, P. (2015). Characterization of DNA in cell culture supernatant by fluorescence-detection size-exclusion chromatography. *Analytical and Bioanalytical Chemistry*, 407(14), 4173–4181. <https://doi.org/10.1007/s00216-015-8639-9>
- Tree, J. A., Richardson, C., Fooks, A. R., Clegg, J. C., & Looby, D. (2001). Comparison of large-scale mammalian cell culture systems with egg culture for the production of influenza virus A vaccine strains. *Vaccine*, 19(25), 3444–3450. [https://doi.org/10.1016/S0264-410X\(01\)00053-6](https://doi.org/10.1016/S0264-410X(01)00053-6)
- Vajda, J., Weber, D., Stefaniak, S., Hundt, B., Rathfelder, T., & Müller, E. (2016). Mono- and polyprotic buffer systems in anion exchange chromatography of influenza virus particles. *Journal of Chromatography A*, 1448, 73–80. <https://doi.org/10.1016/j.chroma.2016.04.047>
- van Wielink, R., Kant-Eenbergen, H. C. M., Harmsen, M. M., Martens, D. E., Wijffels, R. H., & Coco-Martin, J. M. (2011). Adaptation of a Madin-Darby canine kidney cell line to suspension growth in serum-free media and comparison of its ability to produce avian influenza virus to Vero and BHK21 cell lines. *Journal of Virological Methods*, 171(1), 53–60. <https://doi.org/10.1016/j.jviromet.2010.09.029>
- Wang, H., Guo, S., Li, Z., Xu, X., Shao, Z., & Song, G. (2017). Suspension culture process for H9N2 avian influenza virus (strain Re-2). *Archives of Virology*, 162(10), 3051–3059. <https://doi.org/10.1007/s00705-017-3460-8>
- Yuan, M., Gao, X., Chard, L. S., Ali, Z., Ahmed, J., Li, Y., Liu, P., Lemoine, N. R., & Wang, Y. (2015). Efficient purification of cell culture-derived classical swine fever virus by ultrafiltration and size-exclusion chromatography. *Front. Agr. Sci. Eng.* 2(3), 230–236. <https://doi.org/10.15302/j-fase-2015071>
- Webby, R. J., & Webster, R. G. (2003). Are we ready for pandemic influenza? *Science*, 302(5650), 1519–1522. <https://doi.org/10.1126/science.1090350>
- Weigel, T., Solomaier, T., Wehmeyer, S., Peuker, A., Wolff, M. W., & Reichl, U. (2016). A membrane-based purification process for cell

- culture-derived influenza A virus. *Journal of Biotechnology*, 220, 12–20. <https://doi.org/10.1016/j.jbiotec.2015.12.022>
- Wolf, M. W., & Reichl, U. (2011). Downstream processing of cell culture-derived virus particles. *Expert Review of Vaccines*, 10(10), 1451–1475. <https://doi.org/10.1586/erv.11.111>
- Wolff, M. W., & Reichl, U. (2008). Downstream processing: From egg to cell culture-derived influenza virus particles. *Chemical Engineering & Technology*, 31(6), 846–857. <https://doi.org/10.1002/ceat.200800118>
- Wolff, M. W., Siewert, C., Hansen, S. P., Faber, R., & Reichl, U. (2010). Purification of cell culture-derived modified vaccinia ankara virus by pseudo-affinity membrane adsorbers and hydrophobic interaction chromatography. *Biotechnology and Bioengineering*, 107(2), 312–320. <https://doi.org/10.1002/bit.22797>
- Wood, J. M., Schild, G. C., Newman, R. W., & Seagroatt, V. (1977). An improved single-radial-immunodiffusion technique for the assay of influenza haemagglutinin antigen: application for potency determinations of inactivated whole virus and subunit vaccines. *Journal of Biological Standardization*, 5(3), 237–247.
- World Health Organization. (2009). *Pandemic influenza vaccine manufacturing process and timeline*. <https://www.who.int/news/item/06-08-2009-pandemic-influenza-vaccine-manufacturing-process-and-timeline>
- Wu, N. C., Zost, S. J., Thompson, A. J., Oyen, D., Nycholat, C. M., McBride, R., Paulson, J. C., Hensley, S. E., & Wilson, I. A. (2017). A structural explanation for the low effectiveness of the seasonal influenza H3N2 vaccine. *PLoS Pathogens*, 13(10), e1006682. <https://doi.org/10.1371/journal.ppat.1006682>
- Wu, Y., Jia, H., Lai, H., Liu, X., & Tan, W.-S. (2020). Highly efficient production of an influenza H9N2 vaccine using MDCK suspension cells. *Bioresources and Bioprocessing*, 7(1), 63. <https://doi.org/10.1186/s40643-020-00352-4>
- Zost, S. J., Parkhouse, K., Gumina, M. E., Kim, K., Diaz Perez, S., Wilson, P. C., Treanor, J. J., Sant, A. J., Cobey, S., & Hensley, S. E. (2017). Contemporary H3N2 influenza viruses have a glycosylation site that alters binding of antibodies elicited by egg-adapted vaccine strains. *Proceedings of the National Academy of Sciences of the United States of America*, 114(47), 12578–12583. <https://doi.org/10.1073/pnas.1712377114>

SUPPORTING INFORMATION

Additional Supporting Information may be found online in the supporting information tab for this article.

How to cite this article: Bissinger, T., Wu, Y., Marichal-Gallardo, P., Riedel, D., Liu, X., Genzel, Y., Tan, W., & Reichl, U. (2021). Towards integrated production of an influenza A vaccine candidate with MDCK suspension cells. *Biotechnology and Bioengineering*, 118, 3996–4013. <https://doi.org/10.1002/bit.27876>